Moment tensor solutions for small and moderate earthquakes in the Ibero-Maghreb region

Daniel Stich
Instituto Andaluz de Geofísica, Universidad de Granada, Granada, Spain

Charles J. Ammon
Department of Geosciences, Pennsylvania State University, State College, Pennsylvania, USA

Jose Morales
Instituto Andaluz de Geofísica, Universidad de Granada, Granada, Spain

Received 27 June 2002; revised 4 November 2002; accepted 4 December 2002; published 14 March 2003.

[1] We applied time domain moment tensor inversion of local and regional waveforms to small and moderate (M_w = 3.5–5.7) shallow earthquakes from the Iberian Peninsula, northern Morocco, and northern Algeria. For the 6+ years period from November 1995 to March 2002 and the previous Network of Autonomously Recording Seismograms (NARS) experiment, moment tensor solutions were obtained for 58 events, considerably increasing the total number of available solutions in the study area. For each event we performed a moment tensor inversion and a double-couple grid search. For simple faulting events the grid search is valuable as a quality test for its ability to reveal potential ambiguities of the solutions and to assess confidence limits of fault plane parameters or principal axes orientation. The computed mechanisms show regional consistency: A large part of the Iberian Peninsula is characterized by normal faulting mechanisms with SW-NE oriented *T* axes. Thrusting and SE-NW compression is dominant in Algeria. In the Alboran Sea, the westernmost part of the Mediterranean, and the transition between both regimes, strike-slip mechanisms dominate with approximately N-S oriented *P* axes. This pattern suggests a regional anomaly characterized by clockwise rotation of the principal horizontal stress orientations. *INDEX TERMS:* 7230 Seismology: Seismicity and seismotectonics; 7215 Seismology: Earthquake parameters; 8164 Tectonophysics: Evolution of the Earth: Stresses—crust and lithosphere; 8150 Tectonophysics: Evolution of the Earth: Plate boundary—general (3040); 9335 Information Related to Geographic Region: Europe; *KEYWORDS:* moment tensor inversion, waveform modeling, stress field, Iberia

Citation: Stich, D., C. J. Ammon, and J. Morales, Moment tensor solutions for small and moderate earthquakes in the Ibero-Maghreb region, *J. Geophys. Res.*, *108*(B3), 2148, doi:10.1029/2002JB002057, 2003.

1. Introduction

[2] The present-day crustal deformation of the Iberian Peninsula, the Maghreb, and the adjacent offshore regions in the Mediterranean and the Atlantic is driven mainly by the NW-SE directed convergence along this part of the African-Eurasian plate boundary [e.g., *Argus et al.*, 1989; *Kiratzi and Papazachos*, 1995; *Jiménez-Munt et al.*, 2001]. Interference from the Iberian microplate as well as the coexistence of compressional and extensional tectonics [e.g., *Andeweg et al.*, 1999; *Calvert et al.*, 2000] complicate the understanding of the collision, and many aspects of the tectonic structure and development of the region remain a mater of debate. The regional seismicity is diffuse and does not delineate clearly the present-day European-African plate boundary south of the Iberian Peninsula [e.g., *Buforn et al.*, 1995]. Earthquakes activity extends well into definitive intraplate settings like northwestern and central Iberia (Figure 1). This broad distribution of seismicity makes earthquakes valuable indicators for the regional stress field whenever their mechanisms can be reliably determined.

[3] Although destructive earthquakes have occurred within the Ibero-Maghreb region, large events are relatively infrequent and the seismicity is characterized by mostly low-to-moderate magnitude (M_w < 5.5) events. Only few of these events are above the thresholds of routine moment tensor projects like the global Harvard centroid moment tensor (CMT) project [e.g., *Dziewonski and Woodhouse*, 1983]), the MedNet regional CMT project [*Morelli et al.*, 2000; *Pondrelli et al.*, 2002], and the ETH Zürich European-Mediterranean moment tensor project [*Braunmiller et al.*, 2002]. Further moment tensor solutions for several moderate events between 1989 and 1994 are given by *Thio et al.* [1999]. Altogether, moment tensor solutions have been available for a total of 19 events over the Iberian Peninsula,

0148-0227/03/2002JB002057$09.00

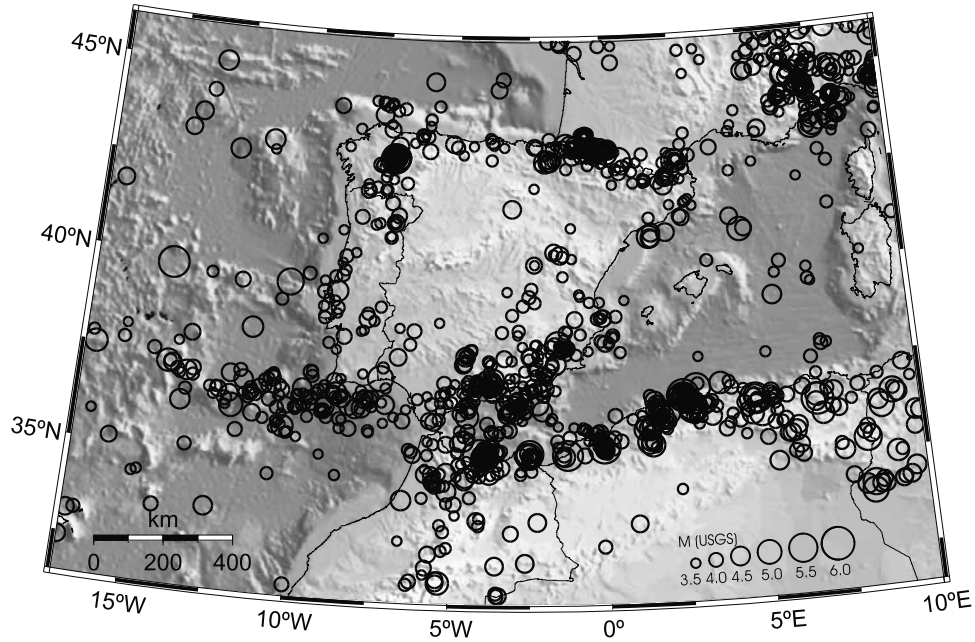

Figure 1. Distribution of small to moderate seismicity in the Ibero-Maghreb region ($m_b \geq 3.5$) for the 20-year period March 1982 to March 2002 (USGS/NEIC data file).

northern Morocco, and the adjacent offshore regions and 21 events in northern Algeria, where larger earthquakes occur more frequently. Additionally, a number of focal mechanisms based on first motion polarities or *P* wave modeling are published (recent work and compilations of mechanisms. e.g., by *Borges et al.* [2001], *Bezzeghoud and Buforn* [1999], *Mezcua and Rueda* [1997], and *Buforn et al.* [1995]).

[4] In this study we expand the Iberian region moment tensor catalogue by modeling seismograms from the more frequent small to moderate (M_w = 3.5 to 5) regional earthquakes. During the last few years several institutes installed broadband seismic stations across the region greatly increasing their total number (Figure 2). For events in recent years the combined networks produce reasonable coverage of most moderate events at local to regional distances. The coverage is suitable for time domain moment tensor inversion to estimate the size, depth, and faulting geometry of these earthquakes. Given our goal to include small events with a reduced number of regional broadband recordings and significant noise level, we emphasized establishing quality criteria to ensure that the least-certain solutions are reliably identified and can excluded from tectonic interpretation. A product of this goal is a procedure to reveal potential ambiguities of the moment tensor solutions for small earthquakes which are roughly simple double couple faulting events: We perform waveform modeling within a dislocation grid search that systematically tests all alternative faulting solutions for compatibility with the data.

2. Selection of Events and Tectonic Setting

[5] We examined a total of 144 events for this study (Figure 2). The analysis of permanent network data starts in November 1995, when four broadband stations operated in the peninsula and one operated in Morocco. The initial earthquake selection includes all events above magnitude m_b = 3.5 reported either by U. S. Geological Survey National Earthquake Information Center (USGS/NEIC), the Instituto Geográfico Nacional (IGN), or the Instituto Andaluz de Geofísica (IAG), except for events before August 1997 and events in Algeria, where the magnitude threshold was m_b = 4.0 (Figure 2). Inspection of signal and noise made clear that the majority of the m_b = 3.5 to m_b = 3.9 events were not suitable for regional waveform inversion with the available data. Still it will be shown that several of them are, especially for recent years which have improved station coverage. We also examined data from the Network of Autonomously Recording Seismograms (NARS) Europe (January 1983 to February 1988) and NARS-Iberian Lithosphere Heterogeneity and Anisotropy (ILIHA) (March 1988 to February 1989) projects when 6 and 13, respectively, temporary broadband stations were deployed on the Iberian Peninsula [*Nolet et al.*, 1986]. At that time, one additional permanent station operated. NARS stations, however, were equipped with a fairly restrictive event trigger and only seven small-to-moderate regional events from 1984 to 1989 produced sufficient recordings.

[6] The geographical distribution of the modeled earthquakes reflects the overall distribution of seismicity in the Ibero-Maghreb region (compare Figure 1): Many of the events are located east of the Gibraltar Arc and spread out diffusely over an ~500 km broad seismic zone centered on the Alboran Sea, containing parts of southeastern Spain and northern Morocco and Algeria. The definition of a linear African-Eurasian plate boundary in this region is a matter of debate [cf. *Jiménez-Munt et al.*, 2001]. West of Gibraltar, most events occur offshore of southern Portugal in the vicinity of the Azores-Gibraltar plate boundary. Further focii of seismicity include northwestern Spain and the Pyrenees. Occasionally events occur in other areas. This widespread seismicity extends over several geotectonic domains with different structure and rheology, thus introducing individu-

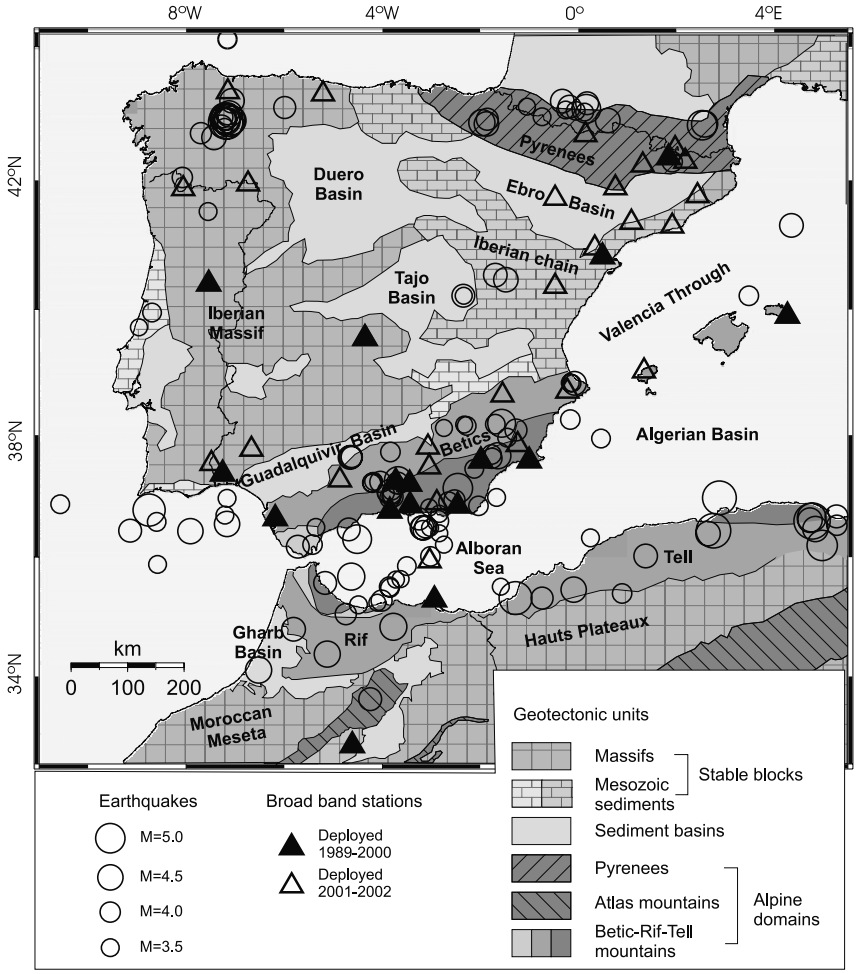

Figure 2. Distribution of the examined events (circles, see text for event selection criteria) and seismic broadband stations (solid and open triangles), as well as a sketch of main geotectonic units, differentiating between stable blocks, basins, and Alpine domains. The open triangles correspond to recently deployed stations that were not yet available for most of the studied events.

ally different local effects onto the propagation properties of seismic waves and the crustal stress field. Hence in this study it is necessary to distinguish between at least three different tectonic environments: stable blocks, Alpine mountain belts, and extensional basins (Figure 2).

[7] Stable blocks, including the Hercynian massif on the Iberian Peninsula, as well as the Moroccan Meseta and the Algerian Hauts Plateaux, are built of deformed Palaeozoic rocks partly covered by Mesozoic sediments. They are only marginally affected by Alpine deformation. Alpine mountain belts, corresponding to thickened crust, are present at the former plate boundary between Iberia and Europe (Pyrenees) and at the present-day contact between Africa and Iberia (Betic-Rif-Tell mountain belt). Internal Cenozoic extensional basins include flexural basins in the foreland of the Alpine belts (Ebro basin south of the Pyrenees, Guadalquivir basin north of the Betics, and Gharb basin south of the Rif), the large internal Tajo and Duero basins, and a number of smaller intramountain basins in both Hercynian and Alpine domains. Further, a regional-scale extensional process is active in the western Mediterranean Sea, manifested in the opening of the Liguro-Provencal basin, the Valencia Through, the Algerian (or South Balearic) Basin east of the Iberian Peninsula, and, since the early Miocene, the Alboran Basin south of Iberia [e.g., *Vegas and Banda*, 1982].

[8] Particularly relevant for the understanding of the plate collision is the Alboran Basin located at the present-day contact between Africa and Eurasia. In the Alboran Basin the continental crust in the internal zones of the Betic-Rif mountain belt has been thinned considerably (crustal thickness in the Alboran Sea of ~15 km compared to >35 km in the central Betics [e.g., *Banda et al.*, 1993; *Casas and Carbo*, 1990]). The transition between the Alboran Basin and the Neogene oceanic crust to the east is gradual [*Torné et al.*, 2000]. The hypocenter distribution of intermediate depth earthquakes [e.g., *Seber et al.*, 1996; *Buforn et al.*, 1995] as well as tomographic images [e.g., *Calvert et al.*, 2000; *Morales et al.*, 1999] indicate the presence of cold and rigid lithospheric material in the sublithospheric upper mantle. Consequently, the formation of the Alboran Basin in a compressional environment may be explained by the removal of subcrustal lithosphere; however, the mechanism is still a matter of debate. Models under discussion include a delamination process [*Docherty and Banda*, 1995; *Seber et al.*, 1996; *Mezcua and Rueda*, 1997], the convective removal of lithosphere [*Platt and Vissers*, 1989; *Calvert et*

Table 1. Summary of Moment Tensor Solutions

Event	Time, UT	Lat, deg	Long, deg	z, m	Moment Tensor Elements,[a] 10^{15} N m						Best Fitting Double Couple (Strike/Dip/Rake)	CLVD, %	Misfit, %	Moment, N m	q
					m_{xx}	m_{yy}	m_{xy}	m_{xz}	m_{yz}	m_{zz}					
840624	1430:52	37.12	−3.70	6	−7.96e−01	−2.80e+01	−1.22e+01	−1.14e+01	−2.02e+01	2.88e+01	166/27/-79, 333/64/-96	18	57	0.39e+17 M_w = 5.0	c
861020B	1448:19	36.78	−8.76	30	1.46e+01	4.50e+00	−5.42e+00	1.10e+01	−1.26e+00	−1.91e+01	255/61/97, 60/30/77	22	70	0.21e+17 M_w = 4.9	b
880708	2331:11	36.21	−5.42	8	3.73e−02	−6.21e−01	1.39e+00	7.01e−01	1.94e−01	5.83e−01	178/61/-159, 78/72/-31	19	46	0.17e+16 M_w = 4.1	c
880725	2003:04	36.55	−7.17	28	3.11e+00	−3.89e+00	−3.80e+00	−1.80e+00	−2.74e−01	7.80e−01	200/70/-7, 293/83/-160;	14	66	0.55e+16 M_w = 4.5	a
881005	0042:11	35.51	−3.86	8	3.61e+00	−4.01e+00	−2.97e−02	1.94e+00	−1.33e+00	3.94e−01	137/59/-173, 43/84/-31	7	52	0.45e+16 M_w = 4.4	c
881031B	1012:58	36.44	2.76	6	1.80e+02	−1.98e+01	−1.64e+02	5.40e+02	−8.48e+01	−1.60e+02	261/80/102, 29/15/39	22	42	0.60e+18 M_w = 5.8	b
890212	1202:19	36.39	2.65	2	2.53e+00	−7.40e−02	−6.87e+00	3.44e+01	−1.67e−01	−2.45e+00	10/11/11, 269/88/101	1	56	0.35e+17 M_w = 5.0	c
951129	0025:08	35.320	−0.740	8	6.55e−01	−7.48e+00	−5.73e+00	5.41e+00	2.28e+00	6.82e+00	2/39/-42, 127/65/-121	27	38	0.11e+17 M_w = 4.7	b
960803	1006:26	40.470	−1.480	10	−6.41e−01	−1.41e−01	−5.47e−01	3.10e−01	−1.85e−01	7.82e−01	146/51/-56, 279/50/-125	7	21	0.98e+15 M_w = 4.0	b
960902	1907:02	37.570	−1.632	10	2.38e+00	−2.96e+00	1.17e−01	2.43e+00	2.79e+00	5.81e−01	44/35/-8, 140/86/-125	7	31	0.46e+16 M_w = 4.4	a
960904	0414:03	36.980	2.880	14	9.50e+01	1.95e+01	−7.54e+01	1.44e+02	−7.35e+00	−1.15e+02	260/70/108, 36/26/49	5	35	0.19e+18 M_w = 5.5	c
961228	0730:36	37.154	−3.713	12	1.99e−01	−6.14e−01	−1.53e−01	−4.40e−01	−4.66e−01	4.15e−01	200/30/-36, 323/73/-115	15	35	0.85e+15 M_w = 3.9	b
970224	0709:50	37.026	−3.834	16	−3.15e−01	−1.45e−01	−1.58e−01	−2.46e+00	−1.55e+00	4.60e−01	302/86/-90, 120/4/-92	3	30	0.29e+16 M_w = 4.3	a
970521B	2350:43	42.880	−7.190	10	5.80e−01	−4.79e+01	−2.80e+01	3.54e+01	3.90e+00	4.73e+01	129/61/-123, 1/42/-46	10	56	0.66e+17 M_w = 5.2	a
970522A	0017:17	42.860	−7.160	8	−1.13e−01	−1.62e+01	−8.48e+00	5.06e+00	6.76e−01	1.64e+01	141/51/-112, 353/43/-65	22	46	0.19e+17 M_w = 4.8	a
970522B	0506:50	42.890	−7.170	10	8.02e−02	−2.54e+00	−1.03e+00	3.03e−01	6.25e−01	2.46e+00	159/52/-93, 343/38/-86	29	33	0.28e+16 M_w = 4.3	b
970702A	0938:41	36.371	−3.235	6	4.96e+00	−5.57e+00	−8.28e−01	2.82e+00	−7.57e−01	6.07e−01	134/68/-165, 38/76/-23	24	57	0.61e+16 M_w = 4.5	b
970702B	1253:05	36.367	−3.255	10	3.96e+00	−4.32e+00	−8.13e−01	1.62e+00	−4.48e−01	3.63e−01	131/73/-167, 38/78/-18	11	32	0.46e+16 M_w = 4.4	a
970702C	1733:05	36.353	−3.243	8	8.63e−01	−8.92e−01	−4.66e−03	3.42e−01	−2.99e−01	2.89e−02	135/63/-178, 44/88/-27	1	37	0.99e+15 M_w = 4.0	a
970703	2023:11	36.362	−3.229	10	8.57e−01	−9.04e−01	−1.31e−01	3.49e−01	6.54e−02	4.72e−02	132/80/-161, 39/72/-10	14	31	0.96e+15 M_w = 4.0	b
970807	1917:26	36.452	−3.238	16	2.50e−01	−2.04e−01	−1.32e−01	2.38e−02	−8.68e−02	−4.57e−02	212/82/20, 119/70/172	17	44	0.28e+15 M_w = 3.6	b
971013	2150:18	36.013	−3.022	4	9.59e−02	−3.92e−01	−4.10e−01	3.27e−01	1.04e−01	2.96e−01	117/71/-133, 8/47/-26	35	38	0.64e+15 M_w = 3.8	b
980406	0011:18	37.012	−1.792	8	5.26e−01	−2.83e−01	−6.20e−01	3.71e−01	2.54e−01	−2.43e−01	21/58/17, 282/76/147	5	35	0.89e+15 M_w = 3.9	b
980413A	0555:41	37.220	−4.260	14	−1.04e−01	2.00e−02	−1.98e−01	8.91e−02	−6.03e−02	8.36e−02	346/61/-21, 87/72/-150	15	59	0.25e+15 M_w = 3.6	b
980413B	1350:52	37.220	−4.278	14	−1.70e−01	7.98e−02	−1.48e−01	9.89e−02	−5.37e−02	8.99e−02	335/55/-20, 77/73/-143	27	50	0.24e+15 M_w = 3.6	b
980414A	0213:03	37.220	−4.210	12	−8.89e−02	8.78e−03	−1.41e−01	6.56e−02	−3.87e−02	8.01e−02	88/69/-145, 344/58/-26	27	52	0.18e+15 M_w = 3.5	b
980717	0829:04	42.870	−7.170	10	−2.67e−02	−7.89e−01	−3.31e−01	3.19e−01	4.90e−01	8.16e−01	152/62/-98, 348/29/-76	15	53	0.11e+16 M_w = 4.0	b
980725	0011:51	40.450	−1.690	20	−1.14e−01	−1.56e−01	−1.52e−01	6.32e−02	1.19e−01	2.69e−01	145/58/-83, 313/33/-100	10	51	0.31e+15 M_w = 3.6	b
981016	0946:46	36.949	−2.643	20	1.67e−01	2.67e−02	−1.62e−01	−6.97e−02	−9.54e−02	−1.94e−01	85/54/131, 209/53/48	4	43	0.27e+15 M_w = 3.6	c
981020	2347:03	34.844	−3.776	6	−3.06e−01	−3.67e−01	−4.25e−01	3.06e−01	−1.14e−01	6.73e−01	116/54/-118, 338/44/-57	9	70	0.79e+15 M_w = 3.9	c

Table 1. (continued)

Event	Time, UT	Lat, deg	Long, deg	z, m	Moment Tensor Elements,[a] 10^{15} N m						Best Fitting Double Couple (Strike/Dip/Rake)	CLVD, %	Misfit, %	Moment, N m	q
					m_{xx}	m_{yy}	m_{xy}	m_{xz}	m_{yz}	m_{zz}					
981114	0309:46	38.210	−0.210	8	3.48e−01	−1.98e−01	−1.03e−01	6.24e−03	2.12e−01	−1.51e−01	42/66/34, 297/59/152	14	43	0.38e+15 M_w = 3.7	c
981118	2318:10	36.990	−3.793	8	−1.13e+00	1.92e−01	−5.41e−01	4.87e−01	7.26e−01	9.34e−01	134/66/-63, 263/35/-135	19	54	0.15e+16 M_w = 4.1	c
981210	1701:09	35.461	−0.097	4	1.85e+00	4.76e−01	−1.37e+00	7.14e−01	−4.02e+00	−2.32e+00	79/24/145, 201/77/70	34	33	0.48e+16 M_w = 4.4	b
990202	1345:17	38.110	−1.490	8	1.15e+01	−1.67e+01	4.75e−01	7.10e+00	−6.37e−01	5.21e+00	41/69/-26, 140/66/-157	8	30	0.17e+17 M_w = 4.8	a
990430	0900:35	39.720	−8.960	16	−3.06e−01	−3.76e−01	−7.59e−01	4.86e−01	−2.52e−01	6.82e−01	348/51/-39, 104/61/-134	3	37	0.11e+16 M_w = 4.0	a
990529	1130:49	36.210	−2.740	6	−5.53e−01	1.24e−01	−3.93e−01	2.74e−01	−2.13e−01	4.29e−01	327/49/-36, 83/63/-133	17	47	0.78e+15 M_w = 3.9	b
990614	2118:30	37.338	−2.174	8	2.00e−01	−1.76e−01	−2.75e−01	−8.91e−02	2.69e−01	−2.45e−02	18/88/41, 287/49/177	7	59	0.44e+15 M_w = 3.7	b
990718	1726:47	35.243	−4.095	10	5.38e−01	−6.50e−01	−4.59e−01	4.23e−01	1.38e−01	1.12e−01	118/83/-149, 24/59/-8	3	50	0.88e+15 M_w = 3.9	b
990804	0902:54	35.575	−5.169	10	−2.47e+00	−2.98e−01	3.02e−01	−9.71e−01	6.45e−02	2.77e+00	263/55/-89, 81/35/-92	18	79	0.28e+16 M_w = 4.3	b
990814	0657:02	38.180	−1.690	6	3.28e−01	−4.28e−01	1.83e−01	−2.49e−01	1.09e−01	1.00e−01	331/57/-169, 235/81/-34	7	36	0.51e+15 M_w = 3.8	a
991004	1814:26	42.900	0.600	10	−1.78e+00	−1.20e−01	−1.14e+00	−1.38e+00	4.96e−01	1.90e+00	141/38/-48, 273/63/-117	2	59	0.26e+16 M_w = 4.2	a
991222	1736:56	35.321	−1.281	8	8.70e+01	1.19e+02	−1.60e+02	1.37e+02	−2.66e+02	−2.06e+02	59/21/118, 209/71/80	22	37	0.38e+18 M_w = 5.7	a
000527	0749:54	36.362	−3.131	16	2.59e−01	−2.64e−01	−1.29e−01	9.79e−02	−2.41e−02	4.62e−03	30/78/-13, 123/77/-167	17	34	0.31e+15 M_w = 3.6	b
000702	0536:24	36.022	1.372	4	8.17e−01	2.58e−01	−1.12e+00	3.93e+00	−3.98e+00	−1.08e+00	68/7/113, 225/83/87	19	59	0.58e+16 M_w = 4.5	c
000705	0926:48	36.448	−7.969	6	1.48e+00	−9.39e−01	−5.17e−01	−2.15e−01	−7.81e−01	−5.38e−01	220/64/26, 117/67/151	6	19	0.16e+16 M_w = 4.1	a
000802	0901:39	37.660	−1.770	4	1.68e−01	2.21e−01	−1.42e−01	−2.25e−01	9.22e−02	−3.88e−01	54/62/102, 210/30/70	30	45	0.44e+15 M_w = 3.7	b
000813	2317:59	35.952	−3.547	14	3.17e−01	−5.47e−01	−2.12e−01	2.96e−01	1.88e−01	2.30e−01	130/75/-138, 27/49/-19	29	53	0.63e+15 M_w = 3.8	b
000818	1815:06	36.196	4.972	4	−1.67e+00	−1.07e+01	−4.01e+01	1.18e+02	−8.08e+01	1.24e+01	238/88/95, 348/6/20	54	51	0.15e+18 M_w = 5.4	c
000823A	0042:06	35.513	−1.583	6	3.12e−01	4.47e−01	−4.21e−01	5.67e−01	−8.10e−01	−7.58e−01	45/19/99, 216/71/87	7	67	0.13e+16 M_w = 4.0	b
001110A	2010:53	36.601	4.773	6	2.19e+02	9.05e+01	−1.14e+02	3.40e+02	−8.99e+01	−3.10e+02	251/70/97, 51/21/71	15	45	0.46e+18 M_w = 5.7	b
001110B	2209:20	36.618	4.725	4	1.83e+00	−4.18e+00	−2.39e+00	2.37e+01	1.42e+01	2.35e+00	121/88/-98, 16/8/-16	3	64	0.29e+17 M_w = 4.9	b
001116	1133:09	36.658	4.759	4	1.07e+01	−9.92e+00	−4.60e+00	5.74e+01	−1.66e+01	−7.58e−01	254/87/88, 103/3/119	33	69	0.61e+17 M_w = 5.2	c
001128	0331:04	35.631	−3.718	6	2.27e−01	−5.93e−01	−5.50e−02	−4.45e−01	3.02e−01	3.66e−01	212/71/-54, 325/40/-150	28	60	0.75e+15 M_w = 3.9	c
010520	0139:10	42.710	−7.700	12	1.21e−01	−1.99e−01	−3.35e−01	−1.45e−01	1.11e−02	7.78e−02	285/80/-158, 191/68/-11	16	49	0.40e+15 M_w = 3.7	c
010608A	13:47:32	35.497	−3.933	8	6.43e−01	−9.34e−01	−3.24e−01	3.46e−01	−3.22e−02	2.91e−01	128/71/-157, 30/68/-21	19	54	0.95e+15 M_w = 4.0	b
010716	2015:45	38.150	−2.280	8	5.29e−02	3.74e−03	−4.13e−01	5.29e−02	1.26e−01	−5.66e−02	270/73/170, 3/81/18	8	45	0.44e+15 M_w = 3.7	b
010923A	0433:48	38.830	−0.080	8	8.49e−01	−9.02e−01	1.56e−01	5.30e−01	−4.65e−01	5.25e−02	49/89/-39, 140/51/-178	7	46	0.11e+16 M_w = 4.0	b
020204	2009:30	37.091	−2.547	10	−1.13e+00	−1.26e+01	−2.78e+00	−1.07e+00	−5.91e+00	1.37e+01	348/57/-88, 164/33/-93	9	52	0.14e+17 M_w = 4.7	a

[a]Read −7.96e−01 as -7.96×10^{-1}.

al., 2000] and several subduction models with different geometry and time history for the presumed slab [*Blanco and Spakman*, 1993; *Zeck*, 1996; *Lonergan and White*, 1997; *Morales et al.*, 1999].

3. Moment Tensor Inversion

[9] The first-order seismic moment tensor is a comprehensive representation of seismic point sources which leads to a simple linear relationship between the three-component seismograms and a set of Green's functions or fundamental fault responses. We invert for a deviatoric moment tensor using complete seismograms recorded at local-to-regional distances (<1000 km) including the full waveforms of *P*, *S*, Love, and Rayleigh waves. Following *Langston et al.* [1982], the best solution is defined to minimize the L2 norm (least squares) of the misfit between observed and predicted waveforms. Hypocenter coordinates are taken from the catalogues of the USGS/NEIC, IGN, or IAG, depending on the event location. The depth is not fixed because it is often not well resolved and has major influence on the expected propagation effects. Instead, a grid search over depths from 2 to 30 km with 2-km increments is performed to obtain the best fitting combination of depth and moment tensor. An application of this inversion technique to the M_w = 4.8, 1999 Mula, Spain, earthquake (990202 in Table 1) is described in detail by *Mancilla et al.* [2002].

[10] Green's functions for the inversion were computed with a reflectivity code [*Kennett*, 1983; *Randall*, 1994] that gives complete far-field solutions for a layered half-space. We assume spatial and temporal point sources since our bandwidth is dominated by periods longer than 10 s. To take into account some important lateral variation of crustal parameters within the study area, three different models are used for different tectonic environments: (1) the Alboran Sea, and offshore conditions in general, (2) the Alpine mountain belts, and (3) the Hercynian basement and Mesozoic platforms. Initially, the models were derived by simplifying and averaging a selection of local and regional Earth models [e.g., *Banda et al.*, 1993; *Carbonell et al.*, 1998; *Du et al.*, 1998; *Gallastegui et al.*, 1997; *ILIHA DSS Group*, 1993; *Téllez and Cordoba*, 1998; *Torné and Banda*, 1992; J. Julià and J. Mejía, unpublished manuscript, 2002]. The models were optimized iteratively by trial and error, calculating Green's functions and inversions for a set of test events. The final models (Figure 3) usually allow sufficient predictions of body and surface waveforms for periods as short as 10 s within geologically uniform regions and distances <200 km and periods as short as 20 s for almost the entire study area. Note that the Alboran model is not actually a model of the offshore lithosphere but averages offshore and onshore properties for paths with sources in the Alboran Sea or northern Algeria and receivers onshore, preferably near the coast. For predominately continental propagation paths the Hercynian basement model usually predicts waveforms the best. The choice between the Hercynian and the Alpine models is less crucial, but the Alpine model tends to perform better for paths predominately within the Betic Chain.

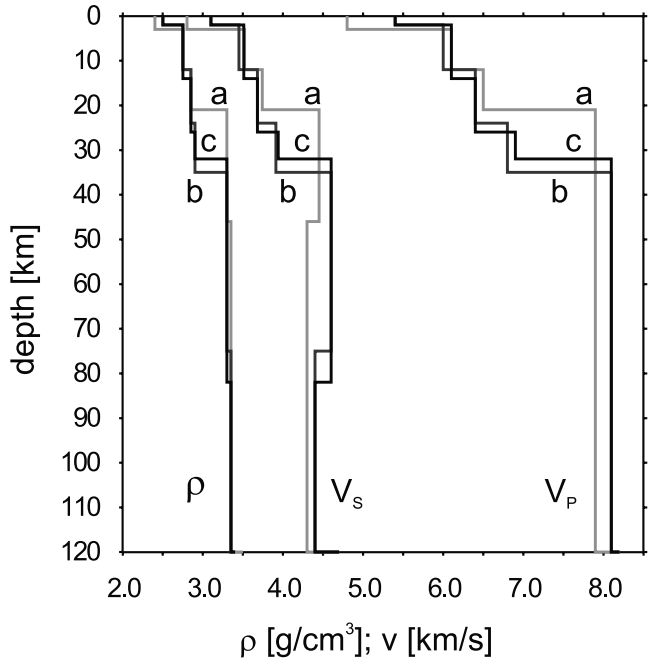

Figure 3. Variation of density, *S* wave velocity, and *P* wave velocity with depth (from left to right) for the layered Earth models used in this study. Model *a* was derived for the Alboran Sea and western Mediterranean, model b for the Alpine mountain belts and model c for the Hercynian basement, Mesozoic platforms or mixed propagation paths.

[11] Prior to inversion, the waveforms are corrected for the respective instrument responses, band pass filtered and aligned with the Green's functions at the *P* arrival. The alignment minimizes the influence of location errors and Green's functions' inaccuracies. The filter band is individually adjusted to data characteristics and quality, typical filter bands are 50 to 20 s for events with $M_w > 4$, and 35 to 15 s for smaller events. Recording stations with high noise level or inappropriately corrected propagation effects are excluded from the inversion, but their predictions are still calculated to confirm a basic compatibility with the obtained moment tensor solution. Usually the remaining waveforms are not weighted for the inversion since the observed amplitudes already give an appropriate distance-dependent weighting, enhancing the influence of short distance recordings with less noise and, usually, better path corrections. However, sometimes additional weighting is applied to

Figure 4. (opposite) Selected moment tensor inversion results and waveform matches for (a) two moderate event, (b) two events with $M_w \approx 4$, and (c) two smaller events $M_w < 4$. Observed and predicted displacement waveforms are plotted in black and gray, respectively. Traces are radial, transversal and vertical component from top to bottom. Next to the traces, the weighting factors for inversion are annotated. Time windows of 300 s are shown. Displacement is given in meters. The overlay plots are labeled with the station names; to the left, the station distribution is shown in a plan. The moment tensor inversion result is given in lower hemisphere equal-area projection, with the moment magnitude next to the mechanism. A fractional misfit versus depth curve is given, showing the respective moment tensor solutions at each depth along with their percentage of CLVD component. An arrow indicates the selected depth.

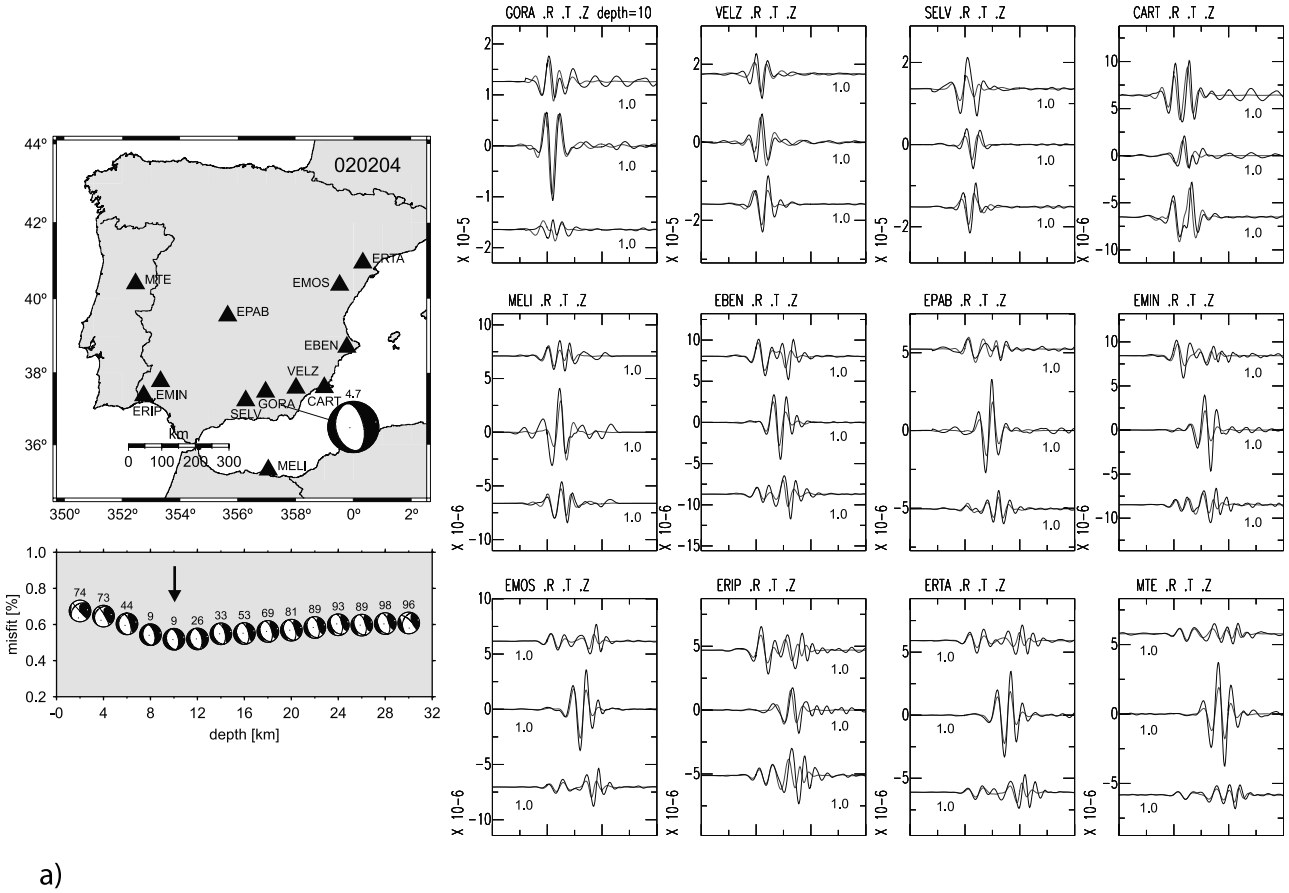
020204
MTE
ERTA
EMOS
EPAB
EBEN
VELZ
EMIN
ERIP
GORA
CART
SELV
MELI
km
0 100 200 300
4.7
misfit [%]
depth [km]
GORA .R .T .Z depth=10
VELZ .R .T .Z
SELV .R .T .Z
CART .R .T .Z
MELI .R .T .Z
EBEN .R .T .Z
EPAB .R .T .Z
EMIN .R .T .Z
EMOS .R .T .Z
ERIP .R .T .Z
ERTA .R .T .Z
MTE .R .T .Z

a)

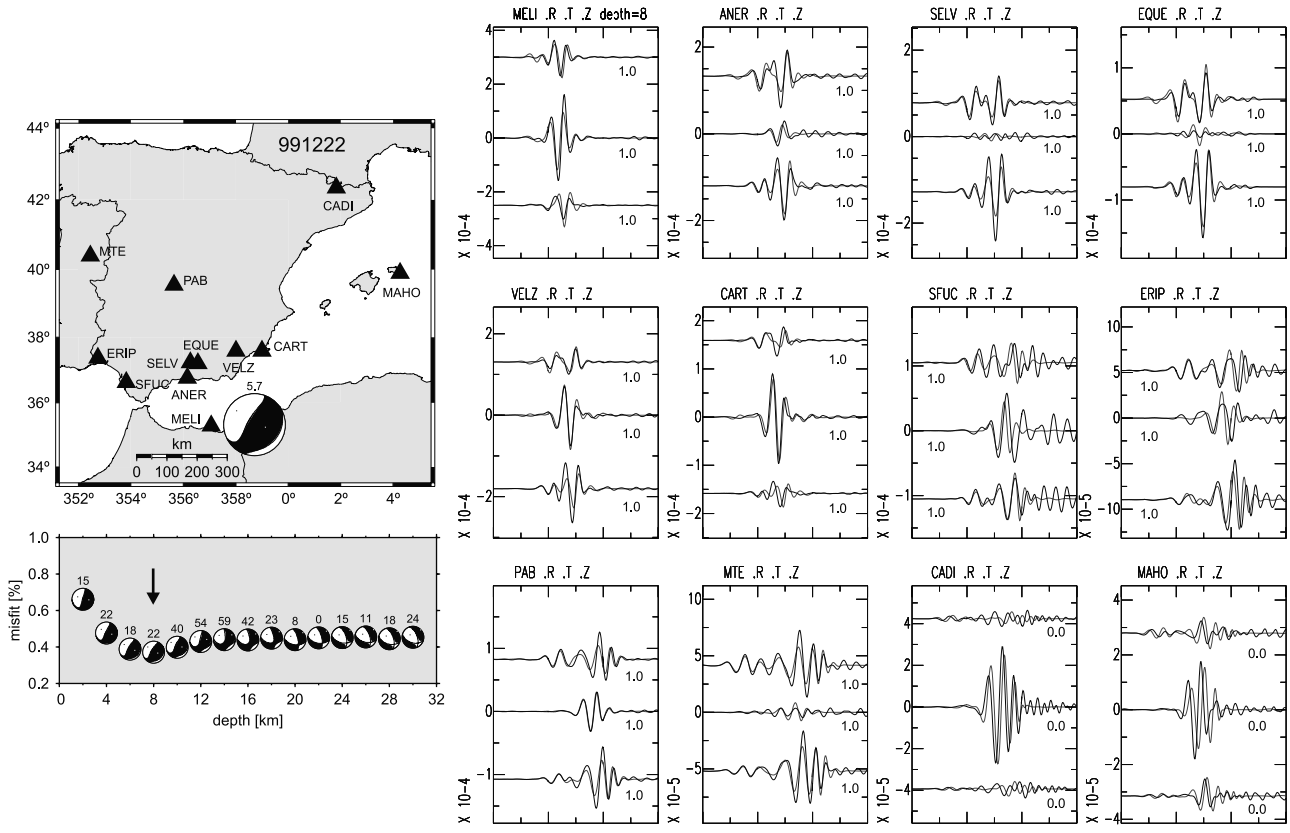
991222
CADI
MTE
PAB
MAHO
ERIP
EQUE
CART
SELV
VELZ
SFUC
ANER
MELI
km
0 100 200 300
5.7
misfit [%]
depth [km]
MELI .R .T .Z depth=8
ANER .R .T .Z
SELV .R .T .Z
EQUE .R .T .Z
VELZ .R .T .Z
CART .R .T .Z
SFUC .R .T .Z
ERIP .R .T .Z
PAB .R .T .Z
MTE .R .T .Z
CADI .R .T .Z
MAHO .R .T .Z

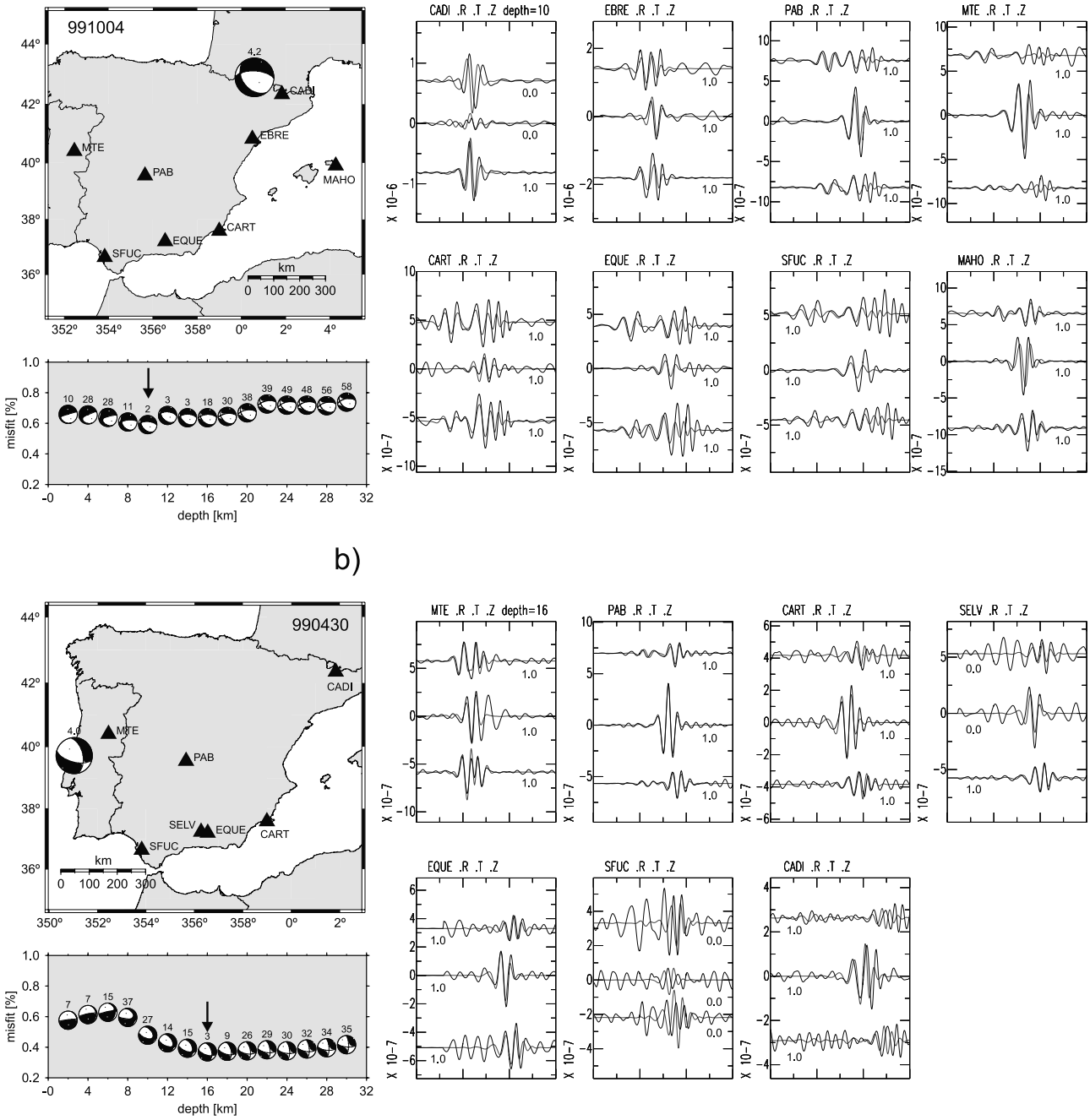

Figure 4. (continued)

individual stations or individual components in order to reduce azimuthal unbalance or alter the relative influence of Love and Rayleigh waves onto inversion. Always several permutations of contributing stations are tested to assure that particular stations do not significantly bias the solution while reducing waveform matches at the remaining stations. This may be caused by data insufficiencies or any major misestimation of propagation effects, e.g., a phase mismatch of large-amplitude surface waves.

4. Discussion of Inversion Results

[12] We computed 58 moment tensors for the Ibero-Maghreb region. For 44 of these events no moment tensor solutions have been available previously. The inversions involve waveforms at 3 to 12 stations each. The use of a single misfit measure (least squares misfit) is convenient, but a great simplification of the information contained in the seismograms. To include information on the reliability of the inversion results using additional information than the simplified misfit, we classify each solution considering a number of quality criteria outlined below. To illustrate the scope of the moment tensor inversion in the region, we first discuss selected inversions in detail, analyzing the waveform matches of *P*, *S*, and surface waves between observed and predicted seismograms. To obtain a representative selection, we choose two events each from three magnitude ranges ($M_w \geq 4.5$, $M_w \approx 4$, and $M_w < 4$) (Figure 4). The

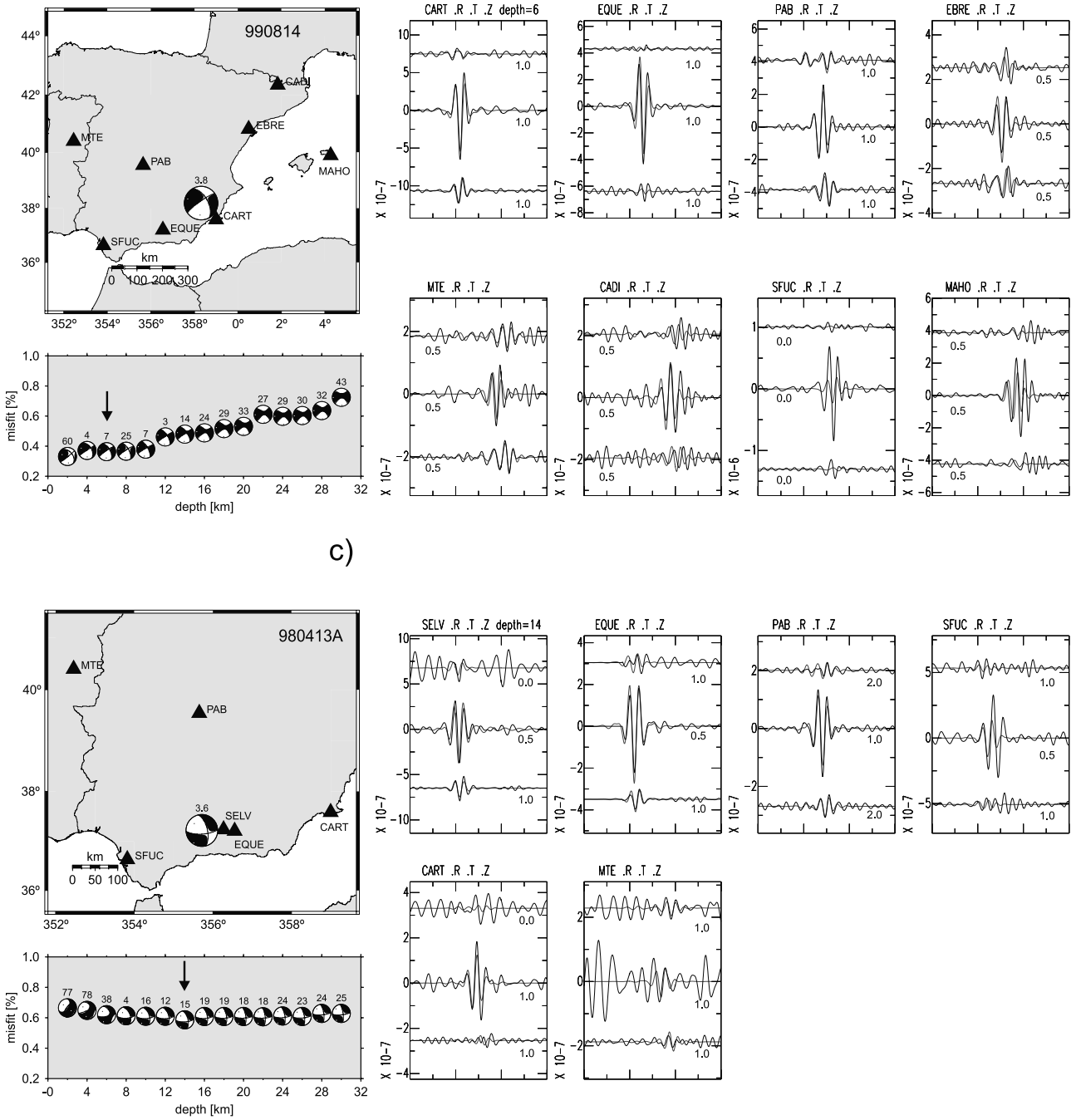

Figure 4. (continued)

selected events include examples from different geographic and tectonic regions: intraplate Iberia, Betic Range, Pyrenees, and northern Algeria. The events are identified with numbers listed in Table 1.

4.1. Earthquakes With $M_w \geq 4.5$

[13] For the selected moderate events in northwestern Algeria (991222, M_w = 5.7) and southeastern Spain (020204, M_w = 4.7), high-quality regional seismograms at 12 stations each are used for inversion. The traces are filtered with a passband between 50 and 20 s, where the influence of structural heterogeneity is relatively low. The Hercynian basement model has been chosen for modeling, except for stations CADI and MAHO for event 991222 where the long offshore paths make the Alboran model more appropriate. The good waveform matches at all stations suggest that both the inverted mechanisms and the correction of propagation effects are accurate for these events. For both events the solutions agree with the results given by routine moment tensor projects, see below. In any case, the Algerian earthquakes are some of the most difficult for us to constrain because they effectively lie on the edge of our network and our azimuthal coverage for those events is limited.

4.2. Earthquakes With $M_w \approx 4$

[14] Examples of events with $M_w \approx 4$ (Figure 4b), are selected from the Pyrenees (991004, M_w = 4.2) and western Portugal (990430, M_w = 4.0). The traces are of high quality

for most recordings of 991004, but only two stations recorded high signal-to-noise ratios for event 990430. All modeling is done with the Hercynian basement model, again the filter passband is from 50 s to 20 s. For 991004, most waveform fits are good except of CADI and SFUC. We attribute these failures to nonmodeled effects of local complex structure: The wave propagation toward CADI follows the axis of the Pyrenees mountain range and 3-D effects are plausible (off azimuth energy at this stations is also reported by J. Julià and J. Mejía (unpublished manuscript, 2002)). Still, the ratio of Rayleigh to Love (or *SV* to *SH*) amplitudes is matched well by the solution. Amplitudes at SFUC are underpredicted though the phase is correct, which is a common observation at this station for regional events with northeastern or eastern back azimuth [e.g., *Mancilla et al.*, 2002]. For 990430 the synthetics fit the high-quality recordings of MTE and PAB well and are consistent with the observations at all other stations. In particular, the amplitudes of the Love and Rayleigh waves at the noisier stations are well matched. For both events the inversion yields almost pure double couples (2% and 3% CLVD, respectively).

4.3. Earthquakes With $M_w < 4$

[15] Smaller events (M_w = 3.5 to 3.9) are numerous in the study area and hence valuable for seismotectonic interpretation, but their regional recordings are often significantly affected by noise. Usually, an acceptable signal quality can be obtained in the filter band from 35 to 15 s. This makes modeling more sensitive to details of crustal structure and many of these events are not suitable for regional moment tensor inversion with uniform layered Earth models. Still we were able to obtain 21 solutions for that magnitude range, two examples (980413A, M_w = 3.6 and 990814, M_w = 3.8) are given in Figure 4c. Most traces are noisy, but all observable basic waveform characteristics, at 6 and 5 stations respectively, are matched by the moment tensor solutions. On the basis of waveform matches, we chose for 990814 the best depth different than the formally best solution. The depth of event 980413A is not resolved by the inversion due to the lack of Rayleigh waves in the recordings, but the mechanism is fairly stable between 8 and 20 km depth. As one might suspect that the noise biases the solution, it is noteworthy that we can rule out significant effects at least for event 980413A. This event occurred within a seismic series and two accompanying multiplet events with comparable noise level (980413B and 980414A) result in nearly identical moment tensor solutions (compare Table 1).

[16] All moment tensors are listed in Table 1, along with the hypocenter coordinates, seismic moment, total fractional misfit, and the best fitting double couple solution. Total fractional misfits range from 0.2 to 0.8 in this study. The fractional misfit is often not a very comprehensive measure of quality, because on the one hand it is often not sufficiently sensitive to the fit of the body waves with relatively small amplitudes, while on the other hand misfits for small events are often exaggerated by noise at the beginning and the end of the traces (where the predictions are zero). Consequently, to each solution, a more comprehensive but subjective quality value ranging from a to d was assigned, based mainly on the inspection of waveform matches, data quality and station coverage. Qualities a and b correspond to solutions that we consider reliable (44 solutions). Quality c solutions (14 solutions) are best estimates but possibly not accurate and should be interpreted cautiously. Reasons for assigning an event a grade of c include an incomplete fit of some basic features of the waveforms, high noise level, deficient station coverage or certain instability of the solution when varying weighting factors. Solutions with unsatisfactory waveform matches as well as inversions based on less than three stations correspond to quality d and were excluded from any interpretation and are not reported in this paper. This quality rating also includes information gleaned from uncertainty analyses that we present in the next section.

[17] For 14 earthquakes of our catalogue (Table 2), moment tensor focal mechanisms are provided also by the routine moment tensor projects at Harvard, MedNet, and ETH, or in individual studies [*Thio et al.*, 1999; *Dufumier et al.*, 2000; *Mancilla et al.*, 2002]. Magnitudes of these events range from M_w 5.2 to 5.8 in Algeria and from M_w 4.0 to 5.2 in Iberia. The routine projects are based on less dense seismic networks and some of these earthquakes are close to the lower magnitude limits of the individual projects, particularly the Harvard project. For several events (990202, 991004, 000705, 020204) the previously available moment tensors do not agree well with each other and must include wrong solutions. All Harvard CMT inversions are fixed at 15 km depth and, except for event 052197K, the CLVD components are large (31% to 84%). When integrating the results of this study, we find acceptable agreements for 10 events and inconsistency for 4 events. The latter ones are all located in northern Algeria east of 2.5°E, at the edge of network coverage in this study. Those events have been assigned quality c in this study, except for 881031B (quality b). The solutions that agree well with previous studies correspond to qualities a and b and include events from northwestern Spain (970521B, 970522A), the Pyrenees (991004), southeastern Spain (990202, 020204), offshore from southern Portugal (000705) and in northern Algeria (991222, 001110A). Two strike-slip events in the Alboran Sea (970702A, 970703) agree reasonably with the corresponding MedNet solutions, however, indicating a small normal faulting component in this study instead of the previously detected small reverse component.

5. Dislocation Grid Search Modeling

[18] Small to moderate tectonic earthquakes are usually thought as simple shear failure events corresponding to double-couple force systems. Most of the computed moment tensors have small non double couple components (<20% for 42 and <30% for 53 out of 58 events, Table 1) which we consider plausible to be introduced by noise and inaccurate Green's functions. When considering the sign of the intermediate moment tensor eigenvalue to distinguish between mechanisms with predominantly tensional or compressional strain [*Kuge and Kawakatsu*, 1993], we obtain a fairly symmetrical distribution around zero. Assuming simple dislocation sources for these earthquakes, we can use a double-couple grid search over fault plane parameters and depth as a valuable alternative method to obtain the best source mechanism. For each grid point (strike, dip, rake, depth) we calculate synthetic waveforms and obtain the L2 norm (least squares) misfit between these predictions and

Table 2. Comparison of Available Moment Tensor Solutions

Reference	Event[a]	Region	q	OK?	Lat, deg	Long, deg	Best Double C (Strike/Dip/Rake)	CLVD, %	M_W	M_0, N m
	881031B	northern Algeria	b	yes	36.44	2.76	261/80/102; 29/15/39	22	5.8	6.0e+17
HRV	103188B				36.44	2.63	103/55/167; 201/79/36	55	5.6	3.2e+17
Thio et al.	Tipasa				36.40	2.68	105/65/150	–	5.7	–
	960904	northern Algeria	c	yes	36.98	2.88	260/70/108; 36/26/49	5	5.5	1.9e+17
HRV	090496B				37.03	3.03	11/76/-4; 102/86/-166	43	5.5	1.9e+17
	970521B	NW Spain	a	no	42.88	−7.19	129/61/-123; 1/42/-46	10	5.2	6.6e+16
HRV	052197K				42.95	−7.21	136/66/-122; 13/39/-40	13	5.3	1.3e+17
	970522A	NW Spain	a	no	42.86	−7.16	141/51/-112; 353/43/-65	22	4.8	1.9e+16
MedNet	R052297B				42.85	−7.35	145/68/-105; 359/27/-58	3	4.8	2.3e+16
	970702A	Alboran Sea	a	no	36.37	−3.24	134/68/-165; 38/76/-23;	24	4.5	6.1e+15
MedNet	R070297A				36.36	−3.28	308/68/173; 40/83/22	28	4.5	7.1e+15
	970703	Alboran Sea	b	no	36.36	−3.23	132/80/-161; 39/72/-10;	14	4.0	9.6e+14
MedNet	R070397A				36.64	−2.95	120/65/170; 214/81/25	52	4.0	1.2e+15
	990202	SE Spain	a	no	38.11	−1.49	41/69/-26; 140/66/-157	8	4.8	1.7e+16
Mancilla et al.	Mula				38.11	−1.49	54/77/-29; 151/62/-165	72	4.7	1.3e+16
MedNet	R020299A				38.66	−1.64	22/49/41; 262/61/131	35	4.7	1.5e+16
	991004	SW France	a	no	42.90	0.60	141/38/-48; 273/63/-117	2	4.2	2.6e+15
Dufumier et al.	Saint-Béat				42.87	0.64	151/26/-21; 260/81/-115	–	4.4	4.3e+15
MedNet	R100499A				42.89	0.85	238/31/-109; 80/61/-79	9	4.9	2.4e+16
	991222	NW Algeria	a	no	35.32	−1.28	59/21/118; 209/71/80	22	5.7	3.8e+17
HRV	122299E				35.34	−1.45	29/45/67; 240/49/111	84	5.6	3.0e+17
ETH	991222				35.17	−1.22	59/34/106; 221/57/80	24	5.7	4.3e+17
MedNet	R122299D				35.27	−1.27	63/36/116; 212/58/72	34	5.6	3.2e+17
	000705	southern Portugal	a	no	36.45	−7.97	220/64/26; 117/67/151	6	4.1	1.6e+15
ETH	000705				36.43	−7.92	216/73/28; 118/63/161	30	4.1	1.4e+15
MedNet	R070500A				36.44	−7.92	288/36/128; 64/63/66	39	4.1	2.0e+15
	000818	northern Algeria	c	yes	36.20	4.97	238/88/95, 348/6/20	54	5.4	1.5e+17
HRV	081800E				36.12	5.00	6/81/-19; 99/71/-171	31	5.2	7.3e+16
ETH	000818				36.19	4.97	8/87/-20; 99/70/-177	4	5.2	8.2e+16
MedNet	R081800A				36.04	4.88	6/83/-17; 98/73/-172	45	5.1	6.4e+16
	001110A	northern Algeria	b	no	36.60	4.77	51/21/71; 251/70/97	15	5.7	4.6e+17
HRV	111000E				36.45	4.96	64/38/97; 235/52/85	33	5.7	4.3E+17
ETH	001110A				36.43	4.90	57/25/88; 239/65/91	29	5.9	6.8E+17
MedNet	R111000A				36.33	4.70	67/26/101; 235/65/85	4	5.7	4.8E+17
	001116	north Algeria	c	–	36.66	4.76	254/87/88; 103/3/119	33	5.2	6.1E+16
ETH	001116				36.65	4.75	125/84/-138; 29/48/-8	10	5.0	3.2E+16
	020204	SE Spain	a	+	37.09	−2.55	348/57/-88; 164/33/-93	9	4.7	1.4E+16
HRV	020402A				37.20	−2.39	46/66/-76; 195/28/-119	68	4.9	3.0E+16
ETH	020204				37.14	−2.42	343/62/-97; 178/29/-77	16	4.9	3.0E+16
MedNet	R020402A				37.29	−2.52	341/42/-106; 182/50/-77	39	4.7	1.6E+16

[a]The boldface events refer to events listed in Table 1.

the observations. The global misfit minimum indicates the best double-couple-depth combination for this earthquake. For the comparability of moment tensor inversion and dislocation grid search, the same weighting factors are involved.

[19] Further, we can use the grid search for a straightforward error analysis, because it tests the full range of source mechanisms for their compatibility with the observations. This can assess the tightness of the minima, corresponding to confidence limits, and reveal potential ambiguities of the solution. To delimit the range of possible alternative solutions, we use the global misfit minimum of the dislocation grid search as a reference point. Then we consider all those solutions as acceptable, which have fractional misfits <10% above the global minimum. Experience with these data indicates that this is a conservative estimate, since solutions with tolerable waveform matches do fall into this misfit band but many of the included solutions could be discriminated manually because of basic waveform incompatibilities. The results of this analysis are summarized in Figure 5. Moment tensor principal P and T axes are included in Figure 5, as they provide important tectonic information and avoid the ambiguity of fault and auxiliary plane. For the sake of clarity, only the best solutions for each strike, each dip, and each rake value are shown in Figure 5. Those solutions with lower misfits are highlighted using larger dot size for the axis orientation and line width for the fault planes.

[20] The scatter of the alternative mechanisms varies among the individual events (Figure 5), indicating several very well constrained solutions (e.g., 980717, 991004, and 020204), as well as several poorly constrained solutions (e.g., 881005, 981114, and 000702). The latter ones are assigned a quality c in Table 1, regardless of the quality of waveform matches. Good waveform matches, combined with large scatter of the alternative solutions, suggest that the station distribution for the individual event is incapable to constrain the mechanism. Another criterion used to qualify solution reliability is an excessive rotation of the mechanism with depth (e.g., 990529). On the other hand, even some uncertain results are valuable for tectonic interpretation despite of considerable scatter of the alternative fault planes: This is the case whenever the principal axes azimuths are fairly stable (e.g., 980413B and 000705, even if for both events the ratios of horizontal and vertical slip are uncertain). An interesting pattern of alternative solutions can be observed for event 000802, which can minimize the

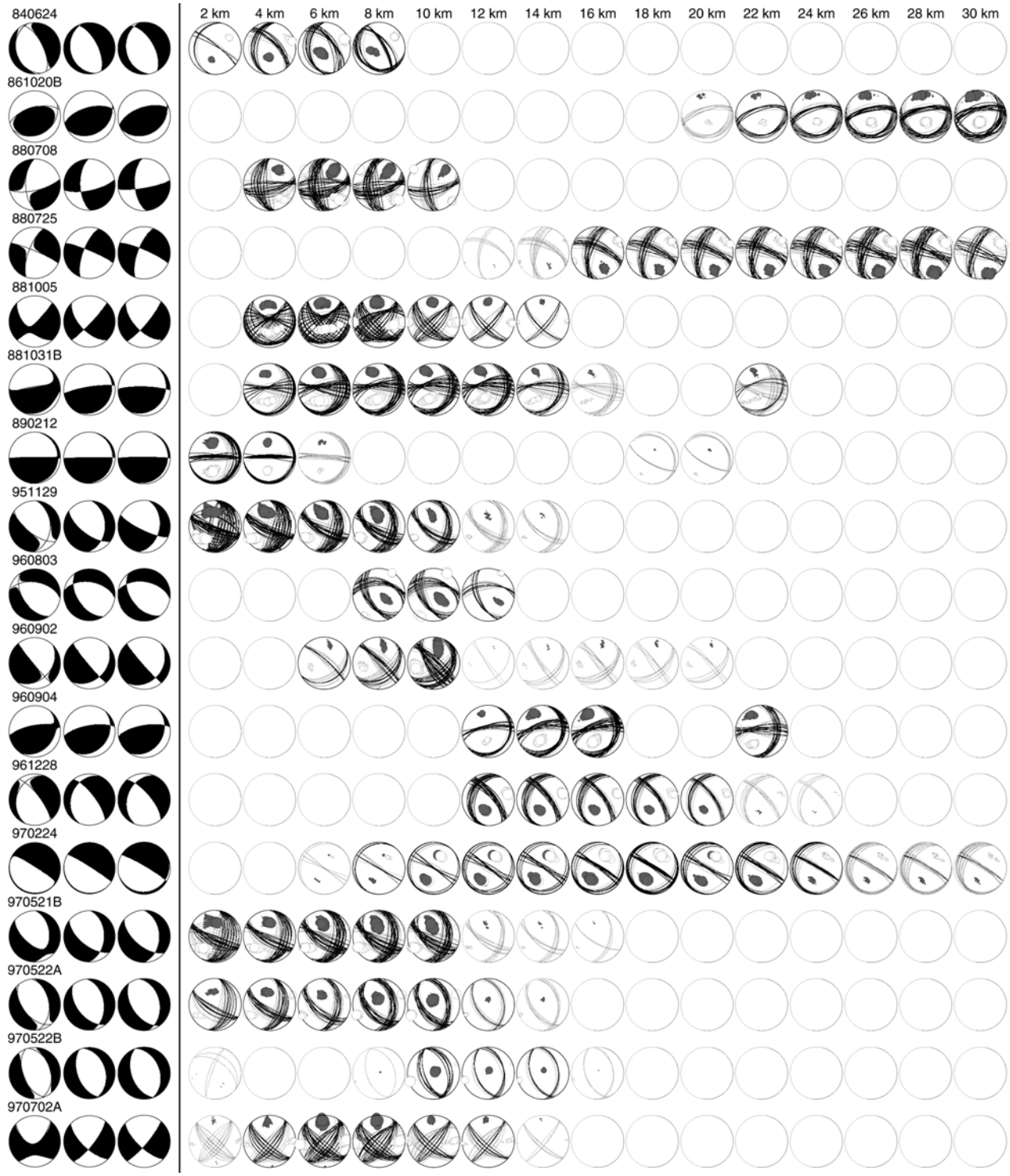

Figure 5. Range of potential alternative solutions as obtained by systematic waveform modeling within a dislocation grid search over fault plane parameters and depth. The scatter of the alternative solutions reflects ambiguities of the inversion result. For the grid an increment of strike, dip, and rake of 10° has been chosen; the depths are spaced 2 km as for inversion. Solutions within the acceptable relative misfit band (global misfit minimum + 0.1, see text) are given. To suppress redundant information, only the best solution for each strike, each dip, and each rake value are shown. For each alternative solution are given the nodal planes and the orientation of the *P* axes (solid dots) and *T* axes (open dots). Line width of the fault planes and size of the stress axis symbols scale linearly with misfit difference. For comparison, the three columns show, from left to right, the preferred moment tensor inversion result, its major double couple, and the best grid search solution. The event identification number according to Table 1 is given above the full moment tensor solutions.

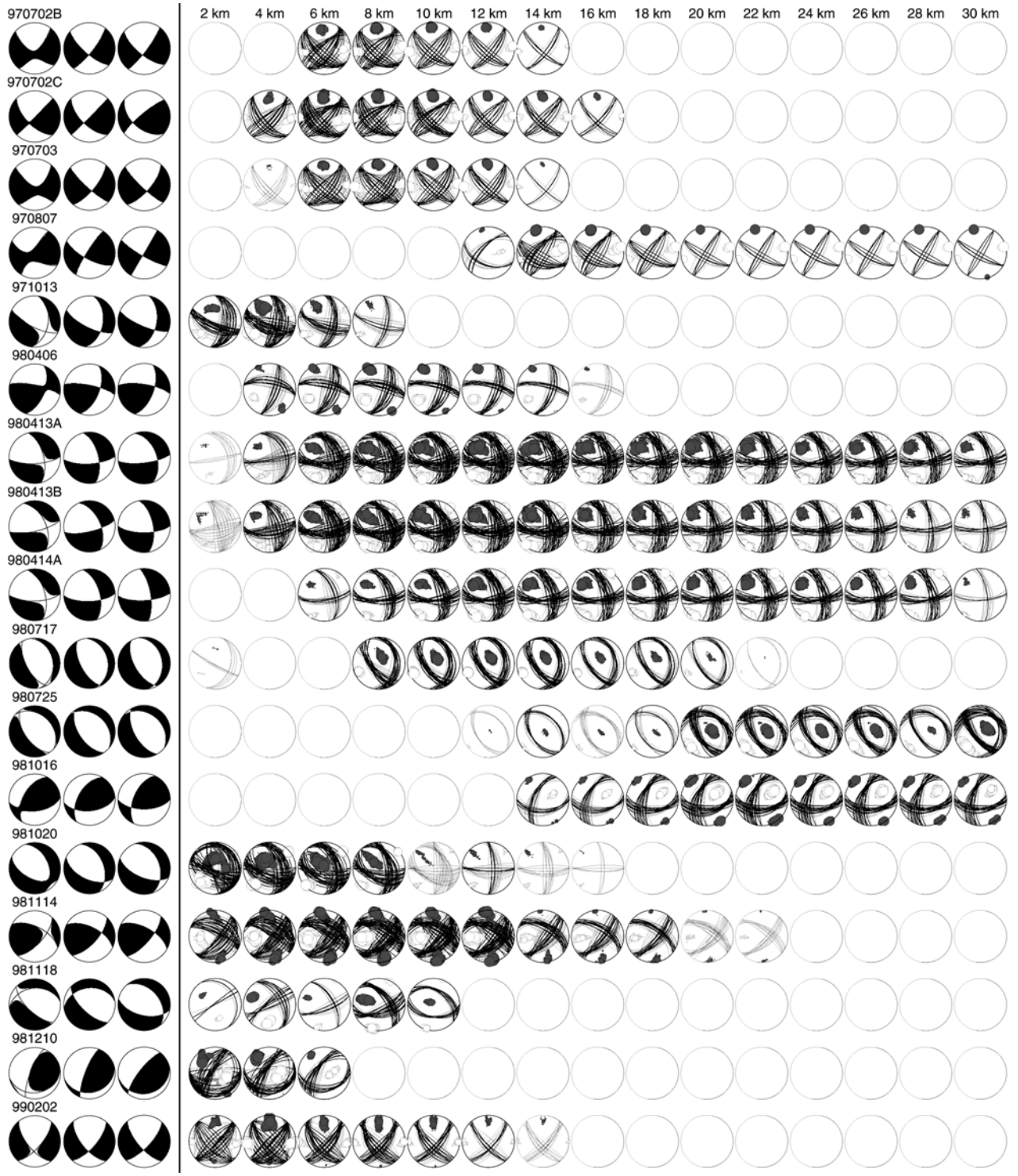

Figure 5. (continued)

least squares waveform misfit norm with both a shallow reverse mechanism and a deep normal mechanism. We can rule out the deep solution since it only predicts the observed large amplitude surface waves but fails to predict amplitude and polarity of the smaller body waves (Figure 6). This is consistent with the network event location that indicates a shallow depth. The event (M_w = 3.7) is a good example for the prudence of our visual inspection and qualitative error assessment.

[21] Apart from the reliability of individual solutions, also global characteristics of the data set are revealed by the dislocation grid search quality test. Generally, the depth resolution from regional long period waveform modeling appears rather low, amounting to ~5–10 km for the majority of events. The resolution of dip and rake is low for many strike-slip earthquakes despite of well constrained strike values and good waveform matches (e.g., 970702A-C, 990202). This is plausible in terms of

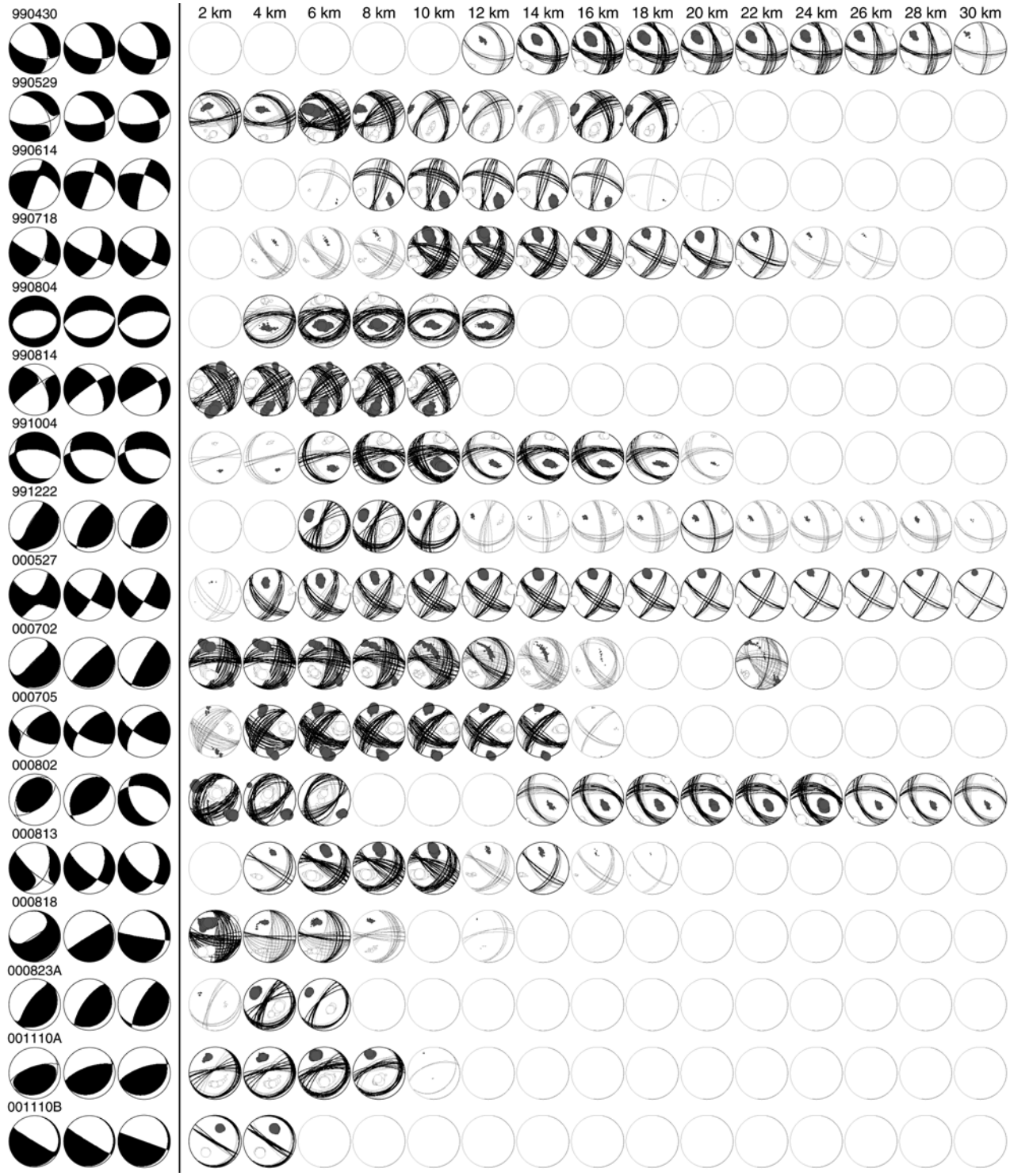

Figure 5. (continued)

radiation pattern similarities for surface waves among the alternative solutions. Earthquakes in Algeria (e.g., 991222, 001110A) are usually characterized by low resolution of strike values, which is plausible because of the limited azimuthal coverage for these events: only for one event (001110B) a nodal plane intersects the station distribution. Finally, for the vast majority of the events, Figure 6 shows the equivalency of the dislocation grid search results and the moment tensor solutions. This confirms our initial assumption that most of these earthquakes are simple faulting events.

6. Regional Consistency of Faulting Solutions

[22] The 58 earthquake mechanisms derived from moment tensor inversion provide a set of stress indicators

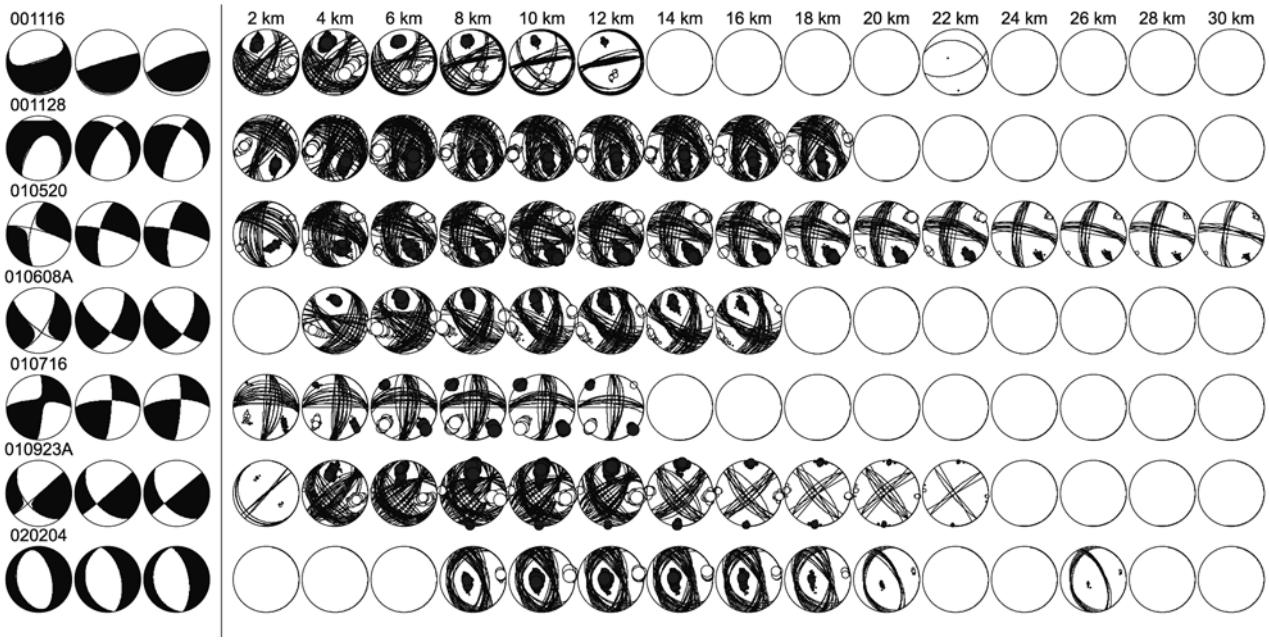

Figure 5. (continued)

for the seismogenic crust, covering both onshore and offshore regions (Figure 7). The solutions are dense in southeastern Spain and the Alboran Sea. The focal mechanisms reveal several clear patterns of faulting within the study area: Mechanisms show great consistency over delimited areas, e.g., northern Algeria and the Alboran Sea. For five regions, we analyze the orientation of faulting solutions: Central and western Iberia, southern Portugal, the Alboran Sea, Algeria, and southeastern Spain. At present, this moment tensor catalogue cannot reveal regional characteristics of faulting in the Pyrenees and northeastern Spain, northern Morocco and the Gibraltar Arc due to a lack of solutions. We proceed region by region and summarize the results in Figure 8.

6.1. Iberia

[23] Over a large part of the Iberian Peninsula, consistent (oblique) normal faulting mechanisms occur, with *T* axes oriented NE-SW (951129, 960803, 970521B, 970522B, 980413A/B, 980414A, 980717, 980725, and 990430). Most of the events included in this region occurred in an intraplate setting outside the zones of major Alpine deformation, except for four events located in the external zones of the Betic Range in southeastern Spain (980413A/B, 980414A, 010716). Two strike-slip events with compatible *T* axes orientations occurred within the region (010520 and 010716). The predominantly normal faulting style and the average *T* axes orientation (∼N50°E) suggest NE-SW extension in the stable part of the Iberian Peninsula.

6.2. Offshore Southern Portugal

[24] Near the southern coast of Portugal, two strike-slip and one reverse mechanism show consistent orientation of the *P* axes in NNW-SSE direction (∼N160°E). Although the regional faulting characteristics are documented by only three mechanisms in this study, the observed faulting style and principal axes orientations are consistent with the previously reported mechanisms along this part of the Azores-Gibraltar plate boundary [*Buforn et al.*, 1988; *Borges et al.*, 2001].

6.3. Alboran Sea

[25] In the offshore parts of the Alboran Basin, mechanisms are predominantly strike-slip with nearly N-S oriented P axes (∼N170°E) and nearly E-W oriented *T* axes (∼N80°E). Most mechanisms include a minor component of normal faulting, consistent with the observed regional extension.

6.4. Northern Algeria

[26] In northern Algeria, reverse faulting with SE-NW (∼N140°E) oriented P axes dominates. We suppose the near horizontal nodal planes of the mechanisms are the active fault planes of shallow thrust events. The fault plane orientations agree with most Harvard CMT, MedNet, regional CMT, and ETH moment tensor solutions for this area. Additionally a number of strike-slip events with similar *P* axes azimuth are reported. From west to east a gradual rotation of the *P* axes' direction is apparent in our data, but we suspect that this may be influenced by limitations of azimuthal station coverage. A mechanism of differing orientation is those of event 001110B, which is an aftershock of event 001110A and supposedly reflects a local stress imbalance caused by the main event.

6.5. Southeastern Spain

[27] Here we include events from the central Betics and the southeastern coast. Focal mechanisms in the region are rather heterogeneous and faulting style ranges from normal (020204) to reverse (000802). Nearby but heterogeneous mechanisms can be observed e.g., in the central Betics in the vicinity of the Granada Basin (840624, 961128, 970224, and 991118 within ∼30 km), in agreement with available local first motion polarity mechanisms [*Galindo-Zaldívar et al.*, 1999], and in the southeast (960902 and 000802 separated by ∼20 km). At the southeastern coast, six events show strike-

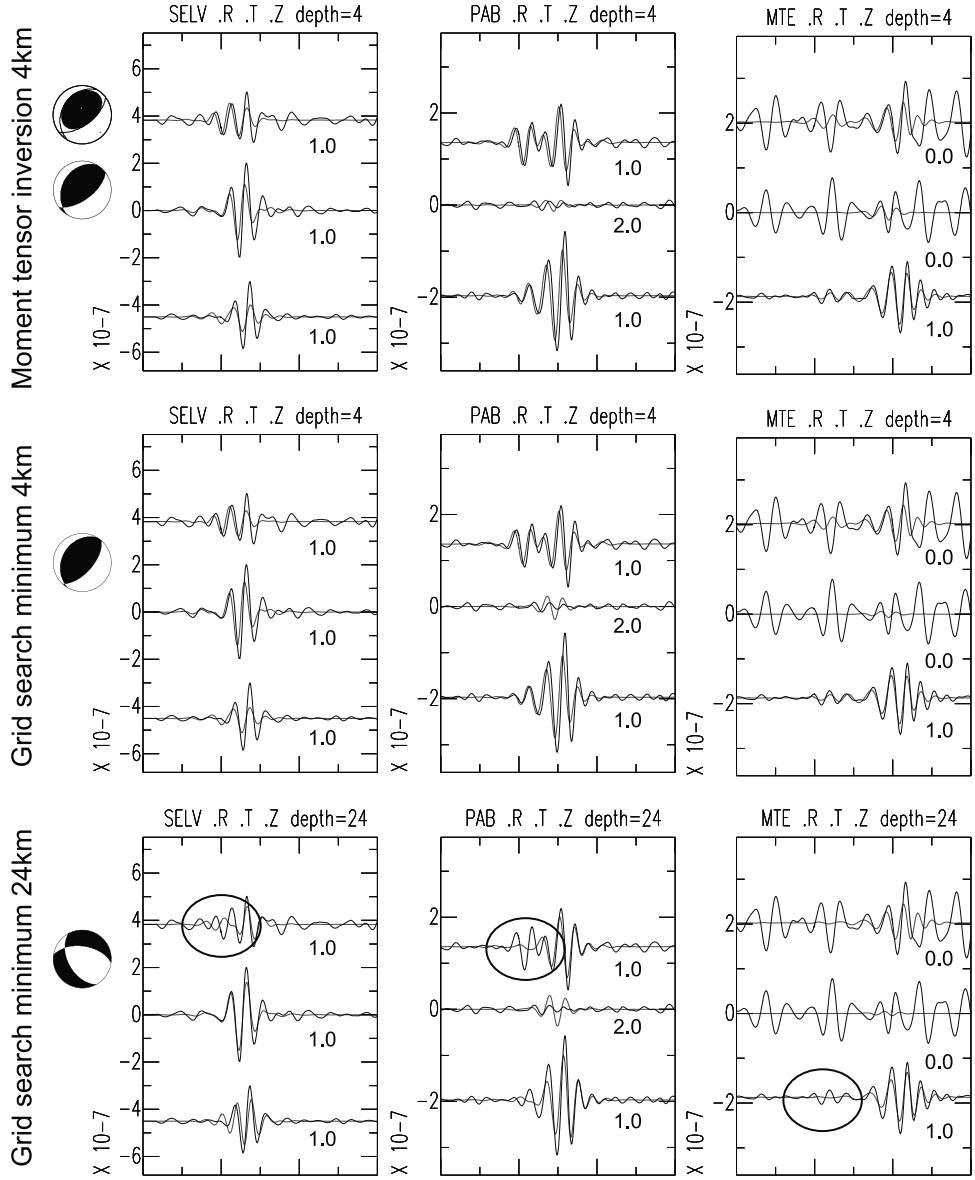

Figure 6. Example for waveform analysis of alternative solutions obtained by the dislocation grid search test: Because of the conservative error estimate, solutions at 4 km (reverse, strike 210°/dip 30°/rake 80°) and 24 km (normal, strike 150°/dip 50°/rake −50°) depth are both included in the range of potential alternative solutions for event 000802, but the deep solution is incompatible with the *P* waves at three stations (the inversion is based on a total of six stations). The best moment tensor solution is shown for comparison.

slip focal mechanisms similar to those in the Alboran Sea (960902, 980406, 981114, 990202, 990814, and 010923A). We consider these strike-slip mechanisms with a nearly north-south (∼N170°E) *P* axes orientation to be characteristic of faulting in the extreme southeast of Spain. In the following, we split the region into an eastern part (east of longitude 2°W, see Figure 8) with predominantly strike-slip mechanisms and nearly north-south oriented *P* axes, and a western region without clearly predominant faulting pattern.

7. Regional Stress Field

[28] The average direction of slip on an earthquake's fault plane depends on the orientation and shape of the stress ellipsoid in the source region. The regional consistency of most earthquake mechanisms in this study suggests that they may be the result of approximately uniform regional stress fields. An individual earthquake mechanism however, as well as a set of nearly identical solutions, cannot constrain the stress tensor since preexisting seismogenic faults are not likely to coincide with present-day planes of maximum shear stress [e.g., *McKenzie*, 1969]. Nevertheless we may expect a correlation between average moment tensor *P*, *T*, and *B* axes directions in a source region, and the maximum, minimum and intermediate principal compressive stresses [e.g., *Zoback*, 1992]. Systematical variations of the dominant faulting regime or the principal axes orientations between source

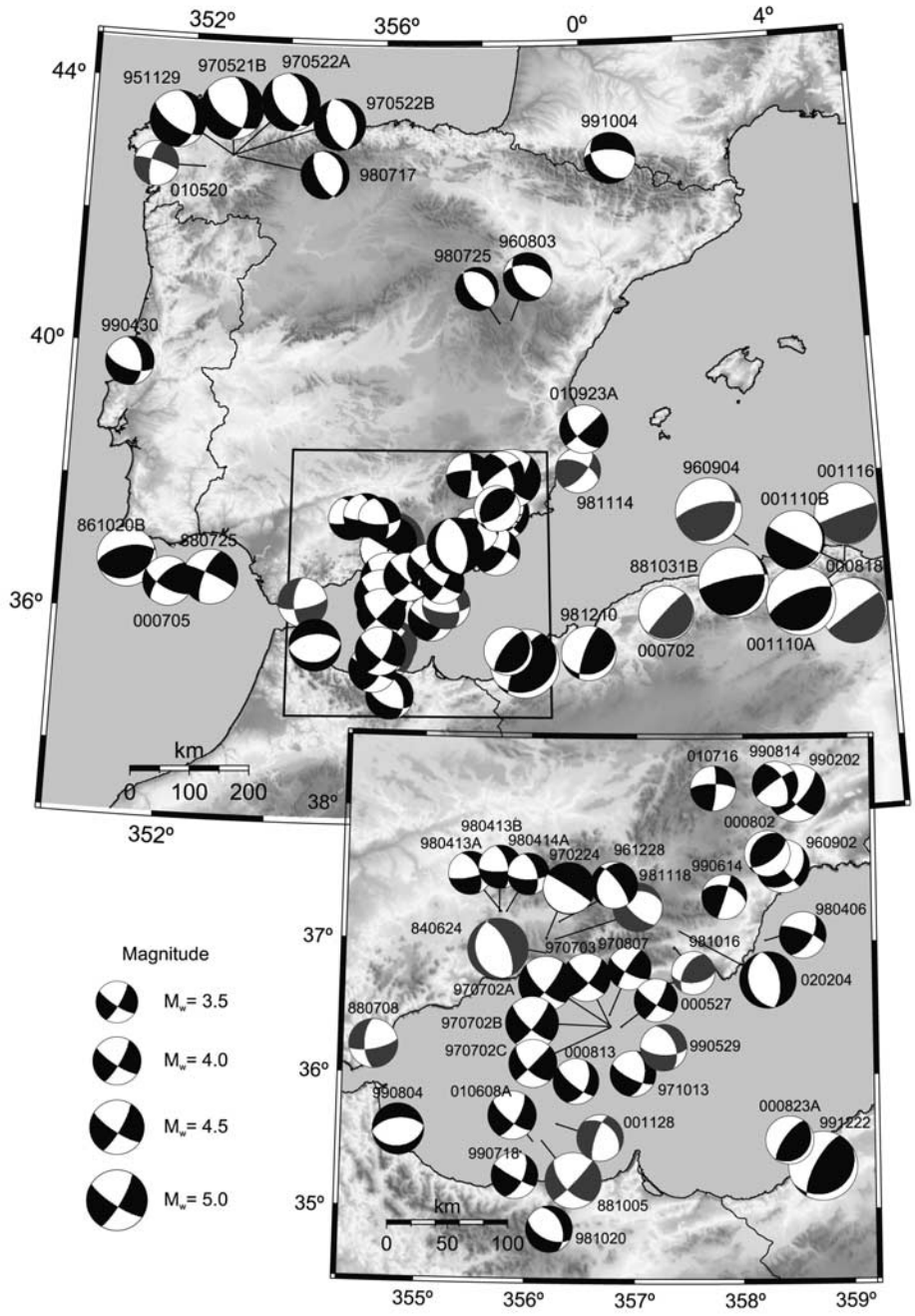

Figure 7. Best double-couple faulting solutions from moment tensor inversion for 58 events in lower hemisphere equal-area projection. The event identification numbers according to Table 1 are labeled at the mechanisms. Mechanism size scales with moment magnitude and is identical for the main map and the enlargement of the Alboran region. The compressional quadrants of quality a and b mechanisms are plotted in black while the less reliable quality c mechanisms are given in gray.

regions should correspond to a change of stress conditions. We assume that the qualitative interpolation of principal axes orientations within and between regions of consistent earthquake mechanisms approximates main regional characteristics of the Ibero-Maghrebian stress field (Figure 8).

[29] Regionally very uniform faulting regimes include normal faulting in large parts of the Iberian Peninsula, strike slip faulting in the Alboran Sea and parts of southeastern Spain and reverse faulting in Algeria. In terms of crustal stress, this corresponds to decreasing relative amplitudes of the maximal horizontal stress respective the vertical stress from Algeria to the Alboran Basin and from the Alboran Basin toward intraplate Iberia. With current seismicity data, we cannot resolve whether these changes of the tectonic regime are gradu-

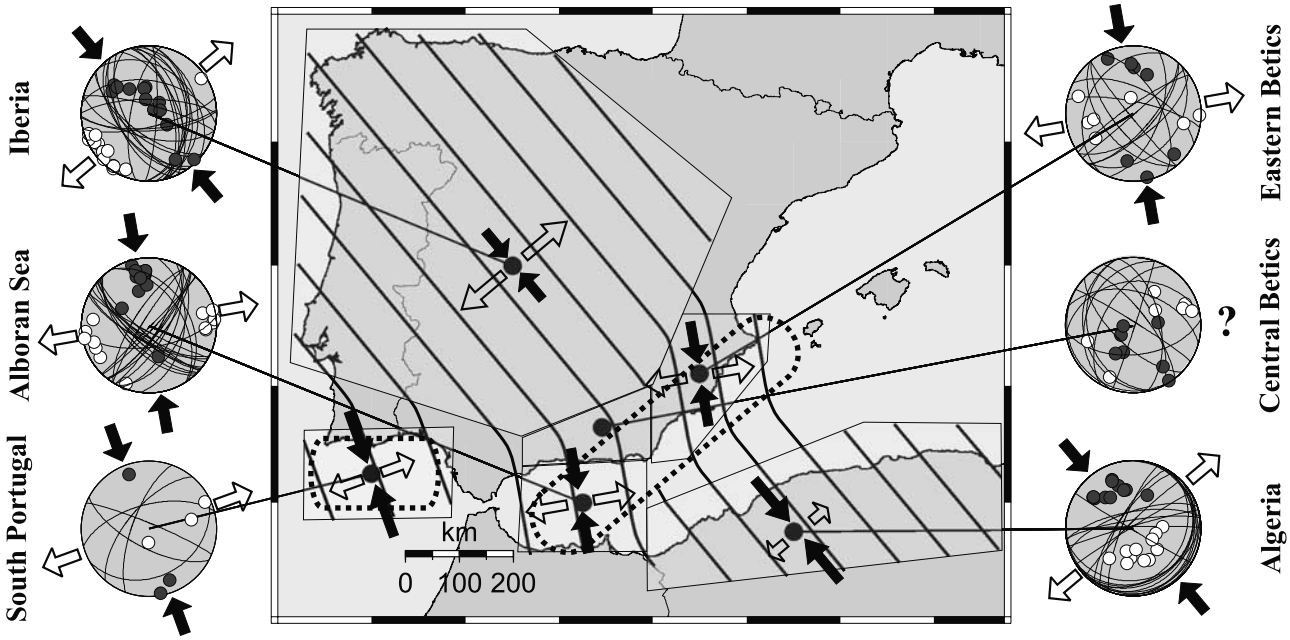

Figure 8. Orientation of nodal planes as well as *P* (solid) and *T* axes (open) for the focal mechanisms from six different regions (regions indicated by shaded boxes). For five regions we can identify a predominant pattern of faulting, the arrows indicate the average orientation of *P* and *T* axes azimuths (black inward pointing arrows for *P*, open outward pointing arrows for *T* axes). Lines are the interpolation of average *P* axes orientations, giving a simplified qualitative approximation to the regional stress field. The dotted lines mark the possible limitations of mayor regional stress anomalies in the Alboran Sea and southeastern Spain, as well as offshore south Portugal.

ally or rather abrupt. In northern Algeria we observe a NW-SE orientation of moment tensor *P* axes in agreement with the direction of convergence along this part of the African-Eurasian plate boundary [*Argus et al.*, 1989; *Jiménez-Munt et al.*, 2001]. Intraplate Iberia is characterized by *T* axes perpendicular to the convergence direction. In intraplate Iberia, a NW-SE orientation of maximal horizontal stress is in agreement with further stress indicators and available stress field inversions [*Herraiz et al.*, 2000; *Mueller et al.*, 2000; *Andeweg et al.*, 1999]. So the stresses in both Algeria and intraplate Iberia appear consistent with the NW-SE regional reference directions associated with the Africa-Eurasian plate convergence.

[30] Striking large-scale anomalies of crustal deformation are reflected in variations in the principal axes orientations in the Alboran Sea, southeastern Spain and south of Portugal (Figure 8). Near the south Portuguese coast, the average *P* axes direction shows a clockwise horizontal rotation of $\sim 20^\circ$ relative to the Iberian data, consistent with further stress indicators provided by *Borges et al.* [2001]. In the Alboran Sea and along the southeastern coast of Spain, the principal axes orientations show an even larger clockwise rotation of $\sim 30^\circ$ relative to the surrounding Iberian-Algerian reference directions. The similarity of source mechanisms within both regions, Alboran and southeastern coastal Spain, suggests that the anomaly is a regional feature, trending $\sim$N50°E from the central Alboran Sea toward the Balearic islands; however, there is no clear evidence whether the anomaly of the Alboran Sea and southeastern Spain is continuous or not. Though we cannot resolve from this study the faulting characteristics in northern Morocco, events 990718 and 981020 suggest that south of the Alboran Basin *P* axes recover their regional NW-SE reference direction. This is supported by further focal mechanisms in previous studies [*Medina*, 1995; *Bezzeghoud and Buforn*, 1999]. Consequently, in the central Alboran Sea the occurrence of a characteristic faulting pattern is apparently limited to a width of $\sim$150 km.

[31] The observed regional variations of faulting mechanisms align with important lateral variations of the lithosphere. The south Portuguese anomaly aligns with the transition between continental and oceanic crust in the Atlantic near probable large strength and density variations [*Borges et al.*, 2001]. The same holds for the anomaly in the Alboran Sea and eastern coast of Spain, which coincides with zones of significant crustal thinning evident in seismic and gravimetric data [*Torné and Banda*, 1992; *Casas and Carbo*, 1990; *Galindo-Zaldívar et al.*, 1998]. In the Alboran Sea the synthesis of heat flow, seismic tomography, and earthquake locations indicates an anomalous mantle with asthenospheric material at shallow subcrustal levels [*Torné et al.*, 2000; *Seber et al.*, 1996; *Calvert et al.*, 2000]. We suggest that lithospheric or sublithospheric processes combine to produce a different style and orientation of faulting compared to surrounding areas and that moment tensor principal axes reflect a rotation of the stress tensor in the Alboran Sea and southeasternmost Spain. The limits of the stress field anomaly, as well as direction and amount of rotation, are possibly constrained by the geometry and

kinematics of the removal of lithospheric mantle in the Alboran Sea.

[32] **Acknowledgments.** We wish to thank our colleagues at the following institutions for collecting and providing seismic broad band data for this study: Geofon, IRIS, ORFEUS, Instituto Andaluz de Geofísica, Instituto Geográfico Nacional, Institut d'Estudis Catalans, Institut Cartogràfic de Catalunya, MIDSEA/Observatori de l'Ebre, Real Observatorio de la Armada, Universidad Complutense de Madrid, and University of Utrecht. We are very grateful for the careful reviews of the original manuscript by Jochen Braunmiller and Luis Rivera. We acknowledge the work on the free software SAC (Seismic Analysis Code [*Goldstein et al.*, 1999]) and GMT (Generic Mapping Tools [*Wessel and Smith*, 1998]). The authors received financial support by the Spanish DGI projects AMB99-0795-C02-01, REN2002-04198-C02-01, REN2001-2418-C04/RIES, by UE-FEDER founds, and within the Research Group RNM104 of Junta de Andalucía. The catalogue of the regional tensor moment solutions can be consulted in the web page of the IAG Regional Moment Tensor Project http://www.ugr.es/∼iag/tensor/.

References

Andeweg, B., G. de Vicente, S. Cloetingh, J. Giner, and A. Muñoz Martin, Local stress field and intraplate deformation of Iberia: Variations in spatial and temporal interplay of regional stress sources, *Tectonophysics*, *305*, 153–164, 1999.

Argus, D. F., R. G. Gordon, C. de Mets, and S. Stein, Closure of the Africa-Eurasia-North America plate motion circuit and tectonics of the Gloria fault, *J. Geophys. Res.*, *94*, 5585–5602, 1989.

Banda, E., J. Gallart, V. García-Dueñas, J. J. Dañobeitia, and J. Makris, Lateral variation of the crust in the Iberian Peninsula: New evidence from the Betic Cordillera, *Tectonophysics*, *221*, 53–66, 1993.

Bezzeghoud, M., and E. Buforn, Source parameters of the 1992 Melilla (Spain, M_w = 4.8), 1994 Alhoceima (Morocco, M_w = 5.8), and 1994 Mascara (Algeria, M_w = 5.7) earthquakes and seismotectonic implications, *Bull. Seismol. Soc. Am.*, *89*, 359–372, 1999.

Blanco, M. J., and W. Spakman, The *P*-wave velocity structure of the mantle below the Iberian Peninsula: Evidence for a subducted lithosphere below southern Spain, *Tectonophysics*, *221*, 13–34, 1993.

Borges, J. F., A. J. S. Fitas, M. Bezzeghoud, and P. Teves-Costa, Seismotectonics of Portugal and its adjacent Atlantic area, *Tectonophysics*, *337*, 373–387, 2001.

Braunmiller, J., U. Kradolfer, M. Baer und, and D. Giardini, Regional moment tensor determination in the European-Mediterranean area: Initial results, *Tectonophysics*, *356*, 5–22, 2002.

Buforn, E., A. Udías, and A. Colombas, Seismicity, source mechanisms and tectonics of the Azores-Gibraltar plate boundary, *Tectonophysics*, *152*, 89–118, 1988.

Buforn, E., C. Sanz de Galdenao, and A. Udías, Seismotectonics of the Ibero-Maghrebian region, *Tectonophysics*, *248*, 247–261, 1995.

Calvert, A., E. Sandvol, D. Seber, M. Barazangi, S. Roecker, T. Mourabit, F. Vidal, G. Alguacil, and N. Jabour, Geodynamic evolution of the lithosphere and upper mantle beneath the Alboran region of the western Mediterranean: Constraints from travel time tomography, *J. Geophys. Res.*, *105*, 10,871–10,898, 2000.

Carbonell, R., V. Sallarés, J. Pous, J. J. Dañobeitia, P. Queralt, J. J. Ledo, and V. García-Dueñas, A multidisciplinary geophysical study in the Betic chain (southern Iberia Peninsula), *Tectonophysics*, *288*, 137–152, 1998.

Casas, A., and A. Carbo, Deep structure of the Betic Cordillera derived from the interpretation of a complete Bouguer anomaly map, *J. Geodyn.*, *12*, 137–147, 1990.

Docherty, C., and E. Banda, Evidence for the eastward migration of the Alboran Sea based on regional subsidence analysis: A case for basin formation by delamination of the subcrustal lithosphere?, *Tectonics*, *14*, 804–818, 1995.

Du, Z. J., A. Michelini, and G. F. Panza, EurID: A regionalized 3-D seismological model of Europe, *Phys. Earth Planet. Inter.*, *106*, 31–62, 1998.

Dufumier, H., A. Souriau, M. Sylvander, S. Judenherc, and M. Granet, Calculs de magnitudes et mécanismes au foyer pour le séisme de Saint-Béat du 4 octobre 1999, *C. R. Acad. Sci.*, *331*, 331–338, 2000.

Dziewonski, A. M., and J. H. Woodhouse, An experiment in the systematic study of global seismicity: Centroid moment-tensor solutions for 201 moderate and large earthquakes of 1981, *J. Geophys. Res.*, *88*, 3247–3271, 1983.

Galindo-Zaldívar, J., F. Gonzalez-Lodeiro, A. Jabaloy, A. Maldonado, and A. A. Schreider, Models of magnetic and Bouguer gravity anomalies for the deep structure of the central Alboran Sea basin, *Geo Mar. Lett.*, *18*, 10–18, 1998.

Galindo-Zaldívar, J., A. Jabaloy, I. Serrano, J. Morales, F. Gonzales-Lodeiro, and F. Torcal, Recent and present-day stresses in the Granada Basin (Betic Cordilleras): Example of a late Miocene-present-day extensional basin in a convergent plate boundar, *Tectonics*, *18*, 686–702, 1999.

Gallastegui, J., J. A. Pulgar, and J. Alvarez-Marrón, 2-D seismic modeling of the Variscan foreland thrust and fold belt crust in NW Spain from ESCIN-1 deep seismic reflection data, *Tectonophysics*, *269*, 21–32, 1997.

Goldstein, P., D. Dodge, and M. Firpo, SAC2000: Signal processing and analysis tools for seismologists and engineers, in *IASPEI International Handbook of Earthquake and Engineering Seismology*, Int. Assoc. of Sesimol. and Phys. of Earth's Inter., Boulder, Colo., 1999.

Herraiz, M., et al., The recent (upper Miocene to Quaternary) and present tectonic stress distributions in the Iberia Peninsula, *Tectonics*, *19*, 762–786, 2000.

ILIHA DSS Group, A deep seismic sounding investigation of the lithospheric heterogeneity and anisotropy beneath the Iberian Peninsula, *Tectonophysics*, *221*, 35–51, 1993.

Jiménez-Munt, I., M. Fernàndez, M. Torne, and P. Bird, The transition from linear to diffuse plate boundary in the Azores-Gibraltar region: Results from a thin-sheet model, *Earth Planet. Sci. Lett.*, *192*, 175–189, 2001.

Kennett, B. L. N., *Seismic Wave Propagation in Stratified Media*, Cambridge Univ. Press, New York, 1983.

Kiratzi, A. A., and C. B. Papazachos, Active crustal deformation from the Azores triple junction to the Middle East, *Tectonophysics*, *243*, 1–24, 1995.

Kuge, K., and H. Kawakatsu, Significance of non-double couple components of deep and intermediate-depth earthquakes: Implications from moment tensor inversions of long-period seismic waves, *Phys. Earth Planet. Inter.*, *75*, 243–266, 1993.

Langston, C. A., J. S. Barker, and G. B. Pavlin, Point-source inversion techniques, *Phys. Earth Planet. Inter.*, *30*, 228–241, 1982.

Lonergan, L., and N. White, Origin of the Betic-Rif mountain belt, *Tectonics*, *16*, 504–522, 1997.

Mancilla, F., C. J. Ammon, R. B. Herrmann, and J. Morales, Faulting parameters of the 1999 Mula earthqake, southeastern Spain, *Tectonophysics*, *354*, 139–155, 2002.

McKenzie, D. P., The relationship between fault plane solutions for earthquakes and the directions of the principal stresses, *Bull. Seismol. Soc. Am.*, *59*, 591–601, 1969.

Medina, F., Present-day state of stress in northern Morocco from focal mechanism analysis, *J. Struct. Geol.*, *17*, 1035–1046, 1995.

Mezcua, J., and J. Rueda, Seismological evidence for a delamination process in the lithosphere under the Alboran Sea, *Geophys. J. Int.*, *129*, 1–8, 1997.

Morales, J., I. Serrano, A. Jabaloy, J. Galindo-Zaldivar, D. Zhao, F. Torcal, F. Vidal, and F. Gonzalez-Lodeiro, Active continental subduction beneath the Betic Cordillera and Alboran Sea, *Geology*, *27*, 735–738, 1999.

Morelli, A., G. Ekström, S. Mazza, S. Pondrelli, E. Boschi, and A. M. Dziewonski, Surface-wave centroid moment tensors in the Mediterranean region: The MEDNET-Harvard project, *Orfeus Electr. Newsl.*, *2*, 1–4, 2000.

Mueller, B., J. Reinecker, O. Heidbach, and K. Fuchs, The 2000 release of the World Stress Map, Res. Group of Heidleberg Acad. of Sci. and Human., 2000. (Available online at www.world-stress-map.org).

Nolet, G., B. Dost, and H. Paulsen, The NARS project: Probing the Earth's interior with a large seismic antenna, *Terra Cognita*, *2*, 17–25, 1986.

Platt, J. P., and R. L. M. Vissers, Extensional collapse of thickened continental lithosphere: A working hypothesis for the Alboran Sea and Gibraltar arc, *Geology*, *17*, 540–543, 1989.

Pondrelli, S., A. Morelli, G. Ekström, S. Mazza, E. Boschi, and A. M. Dziewonski, European-Mediterranean regional centroid-moment tensors: 1997–2000, *Phys. Earth Planet. Inter.*, *130*, 71–101, 2002.

Randall, G. E., Efficient calculation of complete differential seismograms for laterally homogeneous earth models, *Geophys. J. Int.*, *118*, 245–254, 1994.

Seber, D., M. Barazangi, A. Ibenbrahim, and A. Demnati, Geophysical evidence for lithospheric delamination beneath the Alboran Sea and Rif-Betic mountains, *Nature*, *379*, 785–790, 1996.

Téllez, J., and D. Cordoba, Crustal shear-wave velocity and Poisson's ratio distribution in northwest Spain, *J. Geodyn.*, *25*, 35–45, 1998.

Thio, H. K., X. Song, C. K. Saikia, D. V. Helmberger, and B. B. Woods, Seismic source and structure estimation in the western Mediterranean using a sparse broadband network, *J. Geophys. Res.*, *104*, 845–861, 1999.

Torné, M., and E. Banda, Crustal thinning from the Betic cordillera to the Alboran Sea, *Geo Mar. Lett.*, *12*, 76–81, 1992.

Torné, M., M. Fernàndez, M. C. Comas, and J. I. Soto, Lithospheric structure beneath the Alboran Basin: Results from 3D gravity modeling and tectonic relevance, *J. Geophys. Res.*, *105*, 3209–3228, 2000.

Vegas, R., and E. Banda, Tectonic framework and Alpine evolution of the Iberian Peninsula, *Earth Evol. Sci.*, *4*, 320–343, 1982.

Wessel, P., and W. H. F. Smith, New, improved version of the Generic Mapping Tools released, *Eos Trans. AGU*, *79*, 579, 1998.

Zeck, H. P., Betic-Rif orogeny: Subduction of Mesozoic Tethys lithosphere under eastward drifting Iberia, slab detachment shortly before 22 Ma, and subsequent uplift and extensional tectonics, *Tectonophysics*, *254*, 1–16, 1996.

Zoback, M. L., First and second order patterns of stress in the lithosphere: The world stress map project, *J. Geophys. Res.*, *97*, 11,703–11,728, 1992.

C. J. Ammon, Department of Geosciences, Pennsylvania State University, State College, PA 16802, USA. (cammon@geosc.psu.edu)

J. Morales and D. Stich, Instituto Andaluz de Geofisica, Universidad de Granada, Campus Universitario de Cartuja s/n, 18071 Granada, Spain. (morales@iag.ugr.es; daniel@iag.ugr.es)